

# Linking In-Canopy Chemistry to Above-Canopy O<sub>3</sub>, BVOCs, and NO<sub>x</sub> Gas Fluxes in the Amazon Rainforest

Flossie Brown<sup>1,\*</sup>, Colette L. Heald<sup>1,\*</sup>, Allison Steiner<sup>2</sup>, Ana Maria Yáñez-Serrano<sup>3,4,5</sup>, Jürgen Kesselmeier<sup>6</sup>, Carolina de A. Monteiro<sup>7</sup>, Hartwig Harder<sup>7</sup>, Alessandro C. de Araújo<sup>8</sup>, Denisi H. Hall<sup>9</sup>, Cléo Quaresma Dias-Júnior<sup>10</sup>, [Stefan Wolff<sup>6,11</sup>](#)

<sup>1</sup>Institute for Atmospheric and Climate Science, ETH Zurich, 8092 Zurich, Switzerland.

<sup>2</sup>Department of Climate and Space Sciences and Engineering, University of Michigan, Michigan, 48109, United States

<sup>3</sup>Institute of Environmental Assessment and Water Research, IDAEA-CSIC, Barcelona 08034, Spain

<sup>4</sup>CREAF, E08193 Bellaterra (Cerdanyola del Vallès), Catalonia, Spain

<sup>5</sup>CSIC, Global Ecology Unit, CREAF-CSIC-UAB, E08193 Bellaterra (Cerdanyola del Vallès), Catalonia, Spain

<sup>6</sup>Multiphase Chemistry Department, Max Planck Institute for Chemistry, 55128 Mainz, Germany

<sup>7</sup>Department of Atmospheric Chemistry, Max Planck Institute for Chemistry, 55128, Mainz, Germany.

<sup>8</sup>Empresa Brasileira de Pesquisa Agropecuária, Belém, Brazil

<sup>9</sup>National Institute for Amazonian Research, Manaus, AM, Brazil

<sup>10</sup>Federal Institute of Education, Science and Technology of Pará, PA, Brazil

<sup>11</sup>now at: [German Weather Service, 63067 Offenbach am Main, Germany](#)

Correspondence to: Flossie Brown ([flossie.brown@env.ethz.ch](mailto:flossie.brown@env.ethz.ch)) and Colette L. Heald ([colette.heald@env.ethz.ch](mailto:colette.heald@env.ethz.ch))

## 20 Abstract.

The forest canopy is a distinct chemical and dynamical environment compared to the atmosphere above, characterised by natural emissions, deposition processes, and chemistry that vary with height. However, the role of in-canopy chemistry and its influence on above-canopy concentrations of ozone (O<sub>3</sub>) and bi-directional exchange of natural compounds are necessarily simplified within large-scale models. Whilst canopy models have been applied to temperate forests, there are few studies in tropical forests. Here, we apply the FORCAST v2 canopy column model to an Amazonian site. Simulation of the 2015 El Niño shows that biomass burning enhances O<sub>3</sub> flux into the canopy, increases oxidation chemistry and elevates O<sub>3</sub> deposition to vegetation. Sensitivity tests show sesquiterpenes enhance O<sub>3</sub> chemical loss from approximately 3% of the total in-canopy losses to 10%–15%, but only marginally reduce the total canopy O<sub>3</sub> flux. Sesquiterpene canopy escape efficiency varies by 45%–55% across simulations, controlled by O<sub>3</sub> oxidation and vertical turbulence. For other biogenic volatile organic compounds (BVOCs), pool-dependent emissions demonstrate greatest variability in escape efficiency with environmental conditions (monoterpenes 84%–95%, isoprene 95%). Average soil NO<sub>x</sub> escape efficiency (40%–50%) is higher than many existing models suggest and exhibits a strong diurnal cycle that drives O<sub>3</sub> production, especially in the early morning, which may be important to consider in global atmospheric chemistry models. Overall, we highlight reactive BVOCs by inclusion of sesquiterpene emissions and reactivity as major sources of uncertainty in in-canopy chemistry and emphasise the critical role of turbulence in linking canopy processes to above-canopy atmospheric composition.

## 1. Introduction

The Amazon rainforest stretches across 7 million km<sup>2</sup> to form a vast ‘green ocean’ of trees; a continuous canopy of leaves in all directions. This surface plays a pivotal role in tropospheric chemistry, functioning as a dynamic interface that emits biogenic compounds and exchanges trace gases with the atmosphere above (e.g., Covey et al., 2021; Schmitt et al., 2023). Its most significant contributions include biogenic volatile organic compounds (BVOCs) and soil-emitted nitric oxide (NO), both of which influence atmospheric composition and chemistry. These compounds participate in photochemical reactions that lead to the formation of ozone (O<sub>3</sub>), a short-lived climate forcer that adversely affects human health and vegetation. At the same time, O<sub>3</sub> is a key component in maintaining the atmospheric oxidation capacity, thereby regulating the lifetimes of numerous trace gases like BVOCs and methane (CH<sub>4</sub>). These processes contribute to the formation of secondary organic aerosols (SOA), which influence the Earth’s radiative balance and climate system. Furthermore, the forest serves as a surface for the deposition of atmospheric constituents, transferring trace gases from the atmosphere to the ecosystem.

This pristine tropical forest is rapidly changing (Aragão et al., 2018). Human activities and associated climate change are transforming the once-uninterrupted landscape into one fragmented by fire and deforestation (Marengo et al., 2018; dos Reis et al., 2021). From these regions, urban and biomass burning pollution can be advected long distances, influencing the chemical environment far from the emissions source (Brown et al., 2022). In particular, when NO<sub>x</sub> from biomass burning interacts with the rainforest’s naturally high BVOC emissions, it enhances the formation of O<sub>3</sub> (Pacífico et al., 2015; Pope et al., 2020). Elevated O<sub>3</sub>, once transported into the canopy, can enter plant leaves, inhibiting growth and reducing carbon sequestration, threatening the rainforest’s productivity (Cheesman et al., 2024; Vieira et al., 2023). Understanding O<sub>3</sub> concentrations over forested landscapes requires knowledge on how the canopy controls release and uptake of BVOCs, their interaction with NO<sub>x</sub> and the role of the canopy in removing O<sub>3</sub>.

Whilst global models often represent atmosphere-biosphere chemical exchange as a deposition or emission at a single surface layer, below the closed canopy structure exists a chemically vibrant space, with both chemical and depositional transformations occurring before canopy emissions are released to the atmosphere. Beginning in the trunk space, NO emissions from the soil can saturate the lower canopy, reacting with low concentrations of O<sub>3</sub> transported from above (Visser et al., 2022). In the near-perpetual darkness of the closed canopy, this acts as a chemical loss of O<sub>3</sub> and converts NO to NO<sub>2</sub>. As NO is transported vertically, it encounters increasing concentrations of O<sub>3</sub>, VOCs, and their oxidation products, further converting NO to NO<sub>2</sub>. Exchange fluxes of NO<sub>x</sub> and O<sub>3</sub> with soils and trees were intensively studied in the Amazonian rain forest within the LBA project (Gut et al., 2002) confirming that the plant canopy reduces the escape of NO<sub>x</sub> by consumption of NO<sub>2</sub> under the strong influence of stomatal control (Breuninger et al., 2013; Chaparro-Suarez et al., 2011; Gut et al., 2002). Since O<sub>3</sub> and NO<sub>2</sub> are, among several gases, subject to deposition in the canopy and at the soil surface, the canopy acts to reduce the amount of NO<sub>x</sub> from the soil that escapes the canopy at the same time as removing O<sub>3</sub> (Ganzeveld et al., 2002b).

Canopy emission rates in global models are often modified by a species-specific canopy escape efficiency to represent removal within the canopy before release. For soil NO<sub>x</sub>, Yienger and Levy (1995) derive a function based only on leaf area index (LAI)

and stomatal area index (SAI) that implicitly assumes an NO:NO<sub>2</sub> ratio and no temporal variation. However, they highlight that chemistry occurring below the canopy can affect this ratio, and it remains an uncertainty in the parameterisation and assumed magnitude of deposition.

Similarly, O<sub>3</sub> losses within the canopy through deposition and chemistry are often highly parameterised, with chemistry neglected altogether or implicitly included within deposition schemes. At different sites, chemical loss is estimated to contribute anywhere from a minor fraction to 20% of O<sub>3</sub> loss in the canopy (Makar et al., 1999; Rummel et al., 2007; Visser et al., 2021, 2022). In the Amazon, Rummel et al. (2007) cannot explain nighttime chemical losses with soil NO alone and assume a significant contribution from reaction with advected pollutants. Additional research suggests an important role of sesquiterpenes in removing O<sub>3</sub> within the canopy (Isaacman-VanWertz et al., 2024; Jardine et al., 2011; Stroud et al., 2005). These highly reactive BVOC emissions have been measured in the Amazon, with both leaf and soil sources (Bourtsoukidis et al., 2018; Jardine et al., 2011) but are not regularly included in chemistry transport models due to their high reactivity and limited understanding of their chemical products. As these species are considered key to representing the biogenic chemical environment, some studies have included simple sesquiterpene mechanisms (Zhang et al., 2022).

Studies have proposed that accurate representation of NO<sub>x</sub> and O<sub>3</sub> chemistry within the canopy is only possible with explicit canopy resolution. Especially in the tropics, strong gradients in trace gas vertical profiles are formed from low turbulence, allowing stable separation from the boundary layer overnight and in the trunk space (Chamecki et al., 2020; Freire et al., 2017; Serra-Neto et al., 2021). Stratification and the formation of microclimates can further cause processes to deviate from parameterisations. Makar et al. (2017) suggest gradients in light and turbulence within the canopy can reduce above-canopy O<sub>3</sub> concentrations by 12%. Similarly, Visser et al., (2021) find single-layer schemes currently employed by land surface models misrepresent diurnal variability and stomatal:non-stomatal partitioning of O<sub>3</sub> sinks due to missing effects from turbulence. These studies find that only a few layers are needed to improve simulations, suggesting multilayer canopies could be implemented more frequently in global models in the future (Ganzeveld et al., 2002a; Makar et al., 2017; Vermeuel et al., 2024; Wang et al., 2025).

To prioritise development for large scale models, an overview of the factors affecting canopy escape efficiencies and O<sub>3</sub> removal within the tropical forest is required. This includes understanding the role of the above-canopy atmosphere in affecting processes below the canopy, for example through propagation of vertical turbulence or in response to upwind transport of precursors, as well as explicit quantification of the importance of chemistry below the canopy. This study evaluates the role of the canopy in controlling atmospheric composition within and above the Amazon forest using a resolved canopy column model. We compare a year with typical meteorology to one with more extreme conditions including higher fire activity to understand the role of transported pollution on O<sub>3</sub> removal, BVOC escape efficiency and soil NO<sub>x</sub> escape efficiency compared to pristine conditions. This acts as a first step towards identifying the important features of trace gas exchange required for improved representation of tropical forest in-canopy processes and interactions in global models.

Deleted: chemistry

## 2. Methods

### 2. 1. Observation data at the Amazon Tall Tower Observatory

We use the Amazon Tall Tower Observatory (ATTO) site (Andreae et al., 2015) as the location for study and evaluation of  
105 the column model. The site is a research facility within the Uatuma Sustainable Development Reserve, in the pristine Brazilian  
Amazon, 150 km NE of Manaus city (2°S, 59°W). This location is predominantly upwind of the city, although SE–E wind can  
bring pollution from biomass burning and agriculture, especially during the dry season (Pöhlker et al., 2019). The wet and dry  
seasons occur during December–May and July–October, respectively, while November and June are considered transition  
months. Daylight hours are 6:00 to 18:00 local time (UTC-4). The vegetation is old-growth forest, with an average canopy  
110 height of 35 m and greatest leaf density around 25 m (Gomes Alves et al., 2023).

Figure 1a summarises the ATTO measurements used in this study as driving data and for model evaluation. Measurements  
were taken at various heights along the 80 m tower (named the Instant tower, 2.1468° S, 59.0068° W), which has been in  
operation since 2012. Temperature, photosynthetically active radiation (PAR), friction velocity ( $u_*$ ), and wind speed and  
direction measurements are available continuously since 2012 in half-hourly intervals. Relative humidity (RH) in 2013 is also  
115 used for model evaluation.

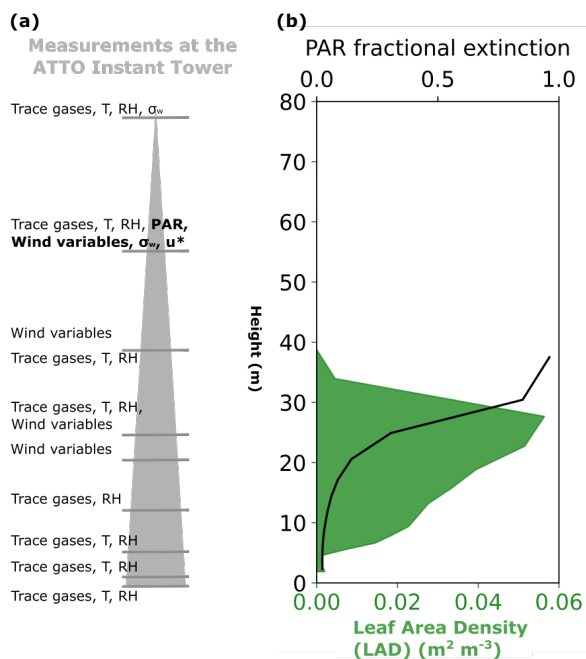


Figure 1: (a) The observed variables used for model evaluation throughout this paper and their approximate measurement heights. Variables measures are trace gases, temperature (T), relative humidity (RH), vertical wind standard deviation ( $\sigma_w$ ), photosynthetically active radiation (PAR), friction velocity ( $u^*$ ) and wind speed and direction (wind variables). Variables in bold are used as driving data in the simulations, (b) prescribed leaf area density (green shading) and fractional extinction of PAR (black solid line) within the canopy (model simulated average). The height scale on both figures is the same.

120

Column model simulations (see Section 2.2) of the ATTO site require forcing data of vertical wind standard deviation ( $\sigma_w$ ),  $u^*$ , PAR, and wind direction which control mixing, temperature and light-related processes. Data from 1–13 November 2013 and 11–23 November 2015 are used in this study; these time periods were selected for maximum meteorological and chemical data availability. Vertical wind standard deviation is not continuously available at the site and was not recorded during 2013. Above-canopy observations are available from an intense campaign in 11–23 November 2015 at 55 m and 81 m. In-canopy observations of  $\sigma_w$  were also measured at 24 m in a shorter period from 11–18 November 2015 (Dias-Júnior et al., 2019).

125

130 November 2013 reflects typical background conditions at ATTO, with moderate temperatures, clean air masses, and biogenic-dominated chemistry, whereas November 2015 represents a perturbed regime characterised by El Niño-driven warming, biomass burning influence, and enhanced atmospheric oxidation (Ribeiro Neto et al., 2022; Silva Junior et al., 2019). Consequently, 2013 observations are representative of the broader atmosphere–biosphere exchange during this period, while 2015 is used to investigate how climate extremes and fire activity may shift the chemical regime. Indeed, November 2015 may be more representative of dry season conditions.

135 To evaluate trace gases in our simulations, we compare model output to observed O<sub>3</sub> concentration measurements taken at the Instant tower during November 2013 and 2015. This profile setup measures at 8 heights using a TEI 49i O<sub>3</sub> analyser (Fig. 1a). The lower part of the vertical profile (0.05, 0.5 and 4 m above the forest floor) was set up on a tripod adjacent to the Instant tower. The upper part of the vertical profile (12, 24, 38, 53 and 79 m) was mounted on the tower. Tubes were guided to a valve system switching every 2 minutes between the different heights during the first three cycles within each hour, and every 1  
140 minute and 30 seconds during the last cycle, resulting in four measurements at each height per hour. The O<sub>3</sub> limit of detection (LOD) is 0.5 ppbv in 60 seconds. There are no O<sub>3</sub> flux measurements available for the simulation period so subsequent evaluations only consider O<sub>3</sub> concentration measurements.

Isoprene, monoterpenes (unspecified) and isoprene oxidation products (MACR, MVK, ISOPOOH) were measured during 5 short campaigns from 2012 to 2015 (Yáñez-Serrano et al., 2015). Measurements were performed with a PTR-MS (Ionicon  
145 Analytic GmbH, Austria) operated under standard conditions using the same profile set up as above (Fig. 1a). As the closest time periods to that of our simulation, we use data from the campaigns in October 2015 and November 2012 as an observational reference to compare to November 2015 and 2013, respectively. Sesquiterpenes have not been measured at the site.

## 2.2. Model description and application to the ATTO site.

We employ the FORCAST v2 model (Ashworth et al., 2015; Wei et al., 2021), a multi-layer column model with explicit canopy  
150 representation originally developed for the University of Michigan Biological Station (UMBS) site. Our set-up includes 18 canopy layers of increasing height, 20 soil layers, and an additional 22 above-canopy layers extending to 5 km. The model timestep is 1 min with output archived every 30 mins. The model is forced by observations at 30 min intervals of wind direction,  $\sigma_w$ ,  $u_*$  and PAR recorded above the canopy (Figs. S1, S2). All other variables including temperature, wind speed, chemistry, water and energy fluxes are prognostic variables in the model after specifying initial conditions. The minimal number of  
155 forcing variables is a feature of this canopy model, since many other canopy chemistry models are nudged by above-canopy observations. Nudging gradually forces model variables towards observations and is commonly applied to constrain above-canopy long-lived gas concentrations and meteorology. This has the advantage of holding the above-canopy environment as close to the true values as possible, which enables evaluation of atmosphere-biosphere fluxes in response to above canopy changes, such as advection. Additionally, the below-canopy environment is more likely to be well-represented and analysis  
160 can focus on below-canopy processes. However, as nudging is a correction rather than an explicit representation of transport, it can mask transport or chemistry errors in the model. To represent lateral transport of air masses in a process-based way,

Formatted: Subscript

Deleted: with the aim that

FORCAST v2 includes an advection parameterisation as a prescribed tendency inside the column. [The advection parameter is adjusted to best reproduce observations of trace gas concentrations.](#) The model is described in detail by Ashworth et al. (2017),

165 Wei et al. (2021) and Bryan et al. (2012). We provide an overview of the model here, and modifications for our application at a tropical site; simulation details and the results can be found in Section 2.3 onwards.

The resolved canopy allows vegetation processes to be computed at each canopy layer. Leaf Area Index (LAI; m<sup>2</sup> leaf area / m<sup>2</sup> ground area) is specified at each layer and PAR is prescribed at the top of the canopy from observations. Canopy structure and radiative transfer properties are specified using parameters to describe the leaf angle distribution and response to incoming  
170 radiation (including absorption, reflection and thermal properties). Each layer is divided into 9 sunlit leaf angle classes and a shaded leaf class, with fractions in each class determined by canopy structure, zenith angle and LAI. Radiation transfer to each layer is calculated using the CUPID model scheme (Norman et al., 1979) allowing calculation of an energy budget. Leaf temperature, latent and sensible heat fluxes are prognostic variables at each layer and for shade and sun leaves in each leaf angle class.

175 For ATTO, LAI (=5.3 m<sup>2</sup> m<sup>-2</sup>) and its vertical distribution at each layer is taken from November 2015 measurements by Gomes Alves et al. (2023) (Fig. 1b). [Variability in LAI at this site is not considered statistically significant \(Botia et al., 2021\).](#) For leaf and canopy parameter values where there are no observations for the tropics, parameters are left in their default state.

#### Emissions

Biogenic emissions are calculated at each layer for each leaf angle class based on PAR (Fig. 1b) and prognostic leaf temperature  
180 of each leaf angle class, and scaled to each layer using LAI in each class.

Synthesis emission fluxes ( $F$ ; nmol m<sup>-2</sup> s<sup>-1</sup>) are calculated by Eq. 1:

$$F = LAI \times \varepsilon_s \times \gamma_{TS} \times \gamma_{LS} \quad (Eq. 1)$$

Where  $\varepsilon_s$  is the light-dependent emission factor at standard conditions of 30°C and incoming PAR of 1000  $\mu\text{mol m}^{-2} \text{s}^{-1}$ , and  $\gamma_{TS}$  and  $\gamma_{LS}$  are scaling factors accounting for the leaf surface temperature and radiation to the leaf. The expressions for  $\gamma_{LS}$   
185 and  $\gamma_{TS}$  are provided in Ashworth et al. (2015) and Guenther et al. (2012).

Pool emission fluxes ( $F$ ; nmol m<sup>-2</sup> s<sup>-1</sup>) are calculated using Eq. 2:

$$F = LAI \times \varepsilon_p \times \gamma_{TP} \quad (Eq. 2)$$

The temperature-dependent pool emission factor  $\varepsilon_p$  (temperature = 30°C) is scaled by  $\gamma_{TP}$  to in response to the leaf surface temperature following Guenther et al. (1995) and described in Ashworth et al. (2015). Species-specific parameter values for  
190 the  $\gamma$  functions are as described in Guenther et al (2012), including the  $\beta$  parameter for temperature dependence (Table 1).

To select the  $\varepsilon_s$  and  $\varepsilon_p$  parameter values at the ATTO site we run 3-day sensitivity studies (Table S1). The short-duration simulation is in-line with previous uses of the model, which were limited to 2-days. The details of the sensitivity tests and comparison to literature are shown in the SI (Figs. S3–S5), with the final parameters included in Table 1. As sesquiterpene emissions are highly uncertain and have the largest impact on O<sub>3</sub> concentrations, we test their contribution to chemistry further  
195 in the main simulations below (Sect. 2.3).

**Formatted:** Font: (Default) Times New Roman, 10 pt, Not Bold, No underline, Font color: Text 1, Pattern: Clear

We set the light-dependent emission factor of isoprene to  $6 \text{ nmol m}^{-2} \text{ s}^{-1}$  to reproduce observed maximum half hourly emissions of  $6\text{--}10 \text{ mg m}^{-2} \text{ s}^{-1}$  at ATTO (Gomes Alves et al., 2023). Other BVOCs (monoterpenes and sesquiterpenes) do not have measured emission fluxes in the Amazon so emission factors must be estimated based on concentrations. We represent  $\alpha$ -pinene as a light-dependent species (Kuhn et al., 2004a, b) and limonene as a temperature-dependent species based on observations at the ATTO site by Yáñez-Serrano et al. (2015), although the light and temperature dependence of tropical species emissions is currently not well characterised. Sesquiterpenes are emitted as 100%  $\beta$ -caryophyllene, given the currently limited understanding of these BVOCs. Sesquiterpenes are considered pool emissions, and the temperature-dependent emissions factor is set at  $0.08 \text{ nmol m}^{-2} \text{ s}^{-1}$  at  $25^\circ\text{C}$  to match observed concentrations from Jardine et al. (2011) (Fig. S3). These measurements were taken at the nearby TT34 tower ( $2^\circ\text{S}$ ,  $60^\circ\text{W}$ ) in the Amazon in 2010 (Jardine et al., 2011) as there are currently no tree- or leaf-level sesquiterpene measurements available at the ATTO site. Recent measurements at the ATTO site indicate that soils and cryptogams are very likely an additional source of sesquiterpenes (Bourtsoukidis et al., 2018; Edtbauer et al., 2021).

Terpenoids react with oxidants  $\text{NO}_3$ ,  $\text{O}_3$  and  $\text{OH}$ ; isoprene dominates  $\text{OH}$  reactivity due to its abundance and some sesquiterpenes demonstrate high reactivity with  $\text{O}_3$ . Comparison of diurnal cycles of  $\text{OH}$  reactivity at 80 m to observations in 2018 by Pfannerstill et al. (2018) show the daily variability of  $\text{OH}$  reactivity is captured by the model, but the model underestimates the magnitude by  $5\text{--}10 \text{ s}^{-1}$ , likely because we do not include a full suite of BVOCs and the simulation length prevents oxygenated products from accumulating (Fig. S6).  $\beta$ -caryophyllene is one of the most reactive sesquiterpenes with respect to  $\text{O}_3$  and it is often measured to be among the most abundant (e.g., Costa et al., 2025; Gomes Alves et al., 2022; Jardine et al., 2011). Thus, by including only this species of sesquiterpene our results represent an upper limit on sesquiterpene  $\text{O}_3$  reactivity.

	Isoprene	$\alpha$ -pinene	Limonene	$\beta$ -caryophyllene
$\epsilon_s$ ( $\text{nmol m}^{-2} \text{ s}^{-1}$ )	6.0	0.4	0.0	0.0
$\epsilon_p$ ( $\text{nmol m}^{-2} \text{ s}^{-1}$ )	0.0	0.0	0.017	0.08
$\beta$ ( $\text{K}^{-1}$ )	0.13	0.1	0.1	0.1

**Table 1: Emission factors used in the simulations for synthesis ( $\epsilon_s$ ) and pool ( $\epsilon_p$ ) emissions selected from sensitivity tests and the  $\beta$  temperature parameters from Guenther et al (2012).**

Soil  $\text{NO}$  emissions are temperature-dependent (Forkel et al., 2006) such that the emission factor ( $0.02 \text{ nmol m}^{-2} \text{ s}^{-1}$ ) is scaled by an exponential dependency on the top layer soil temperature ( $\beta$ ):

$$\beta = e^{0.071 \cdot T(^{\circ}\text{C})} \quad (\text{Eq. 3})$$

Observed soil  $\text{NO}$  emission fluxes in undisturbed tropical forests span a large uncertainty range from 3 to  $100 \text{ } \mu\text{g m}^{-2} \text{ hr}^{-1}$  (Bakwin et al., 1990; Erickson et al., 2002; Lee et al., 2024; Rummel et al., 2002). Most models of soil  $\text{NO}$  estimate values of  $3\text{--}7 \text{ } \mu\text{g m}^{-2} \text{ hr}^{-1}$  (Yan et al., 2005; Yienger and Levy, 1995) for tropical soils. We select an emission factor of  $0.02 \text{ nmol m}^{-2} \text{ s}^{-1}$  for an average emission of  $9 \text{ } \mu\text{gN m}^{-2} \text{ hr}^{-1}$  following sensitivity tests described in the supplementary (Fig. S7). This is at the

225 upper end of previously simulated ranges (Hudman et al., 2012; Yienger and Levy, 1995) as suggested by Lee et al. (2024)  
 but towards the lower end of the large range in observed NO emissions from tropical soils (Lee et al., 2024). Sensitivity tests  
 considering the effect on NO<sub>x</sub> concentrations in comparison to observations at other tropical locations is included in the  
 supplementary (Fig. S7).

230 NO emission fluxes and their sensitivity to driving variables remains a significant uncertainty. Global studies indicate  
 increased emission with temperature (Ke et al., 2022; Luo et al., 2013), however studies on isolated tropical soils tend to show  
 weaker temperature dependence (Cárdenas et al., 1993). Water status is also likely a driving factor of soil NO emission, with  
 limited NO fluxes in water-logged or dry soils and heavy rainfall triggering NO emission pulses (Yienger and Levy, 1995),  
 which is not considered here. There was no rainfall during the simulation periods (Sect. 2.3).

### Deposition

235 Deposition is calculated using a Wesely (Wesely, 1989) resistance scheme, which includes boundary layer ( $R_b$ ), cuticular  
 ( $R_{cut}$ ), mesophyll ( $R_{mes}$ ) and stomatal ( $R_{stom}$ ) resistances at each layer.

Boundary layer resistance follows Gao et al. (1993):

$$R_b = \frac{0.05 \times (lw)^{0.5}}{D} \quad (Eq. 4)$$

240 Where  $lw$  is the leaf width (0.05 m) and  $D$  is the ratio of the gas molecular diffusivity to the molecular diffusivity for water.  
 Cuticular conductance is scaled for each gas type using Henry's law constant ( $H$ ) and reactivity relative to ozone ( $f_0$ ):

$$R_{cut} = \frac{R_{cut0}}{H^{-5} + f_0} \quad (Eq. 5)$$

Using  $R_{cut0} = 1000 \text{ s m}^{-1}$ .

Mesophyll resistance is described using the same predictors:

245 
$$R_{mes} = \frac{1}{\frac{H}{3000} + 100f_0} \quad (Eq. 6)$$

Stomatal conductance uses a Jarvis-type scheme (Jarvis, 1976), which scales a minimum resistance based on empirical  
 sensitivities to meteorological drivers:

$$R_{stom} = R_{min} \times f(T) \times f(PAR) \times \frac{f(VPD)}{f(\psi)} \quad (Eq. 7)$$

250 Where temperature ( $T$ ), PAR, vapour pressure deficit (VPD) and water potential ( $\psi$ ) are calculated for each layer and leaf  
 angle class, using  $R_{min} = 120 \text{ s m}^{-1}$  for H<sub>2</sub>O (and scaled by  $D$  for each gas). These parameter values are in-line with literature  
 and observed values (e.g., Clifton et al., 2023).

Deposition to soil follows Gao et al. (1993) with an additional dependence on surface soil moisture (SM) that rapidly increases  
 resistance in water-logged soils (Eq. 9), described in Ashworth et al. (2015):

255

$$R_{gi} = \left( \frac{H}{R_{gs}} + \frac{f_0}{R_{go}} \right)^{-1} \text{ (Eq. 8)}$$

where  $R_{gs}$  is gas solubility-controlled uptake ( $=500 \text{ s m}^{-1}$ ) and  $R_{go}$  is surface reactivity uptake ( $=200 \text{ s m}^{-1}$ ). In wet soil ( $SM > 0.8$ ):

$$R_{go} = 200 - a(SM - 0.8) \text{ (Eq. 9)}$$

Using coefficient  $a = 1800 \text{ s m}^{-1}$ .

260 Aerodynamic resistance ( $R_a$ ) at the lowest level height  $z$  is defined as:

$$R_a = \frac{z}{K} \text{ (Eq. 10)}$$

These are combined to give a total surface resistance ( $R_g$ ):

$$R_g = R_a + R_{gi} \text{ (Eq. 11)}$$

265

The total deposition velocity ( $v_d$ ) at each layer is transformed into a sink tendency ( $S_{dep} = -\frac{v_d}{z} c \text{ (s}^{-1}\text{)}$ ) using the layer trace gas concentration  $c$  and combined with the emissions tendency before being passed to the vertical transport solver (described below).

Formatted: Font: Italic

Formatted: Font: Italic, Subscript

Formatted: Superscript

Formatted: Font: Italic

### Advection

270

A basic advection scheme must be included for input of nearby heat and trace gas sources since 1-D models do not simulate horizontal atmospheric transport. There is insufficient data at this remote forest site to reliably include a complete mass-balance advection scheme, so FORCAST v2 includes a simple parameterisation based on wind speed and direction developed by Bryan et al. (2012). The advection rate in  $\text{ppbv s}^{-1}$  is proportional to wind speed ( $U$ ;  $\text{m s}^{-1}$ ) scaled by a coefficient  $k$ . The calculation of the  $U$  profile from observed  $u^*$  is described in the SI (Supplementary model description).

275

For the ATTO site, we investigate the inclusion of advection of  $\text{NO}_2$  from biomass burning to heights 73 m – 200 m when the wind direction comes from  $90^\circ - 150^\circ$ . Biomass burning during the southern Amazon dry season (August–October) mostly occurs in the Arc of Deforestation in the E–SE Amazon border, a location named for the agriculture, logging and infrastructure expansion that occurs. Measurements at a site close to ATTO have identified increases of  $\text{NO}_2$  coincident with increases in black carbon, attributed to biomass burning transport from this region (Cordova et al., 2004). Furthermore, back trajectories from HYSPLIT show air masses to the ATTO site arriving from  $90^\circ - 150^\circ$  often originate from biomass burning locations (Pöhlker et al., 2018). Although  $\text{NO}_2$  was not measured, Pöhlker et al. (2018) identify clear increases in biomass burning aerosol when winds arrive from these directions during months August–November. Although November is considered a transition month, biomass burning in the Arc of Deforestation sometimes still occurs. We select a value of  $k$  that best improves representation of observed  $\text{O}_3$  concentrations in 2015 ( $k=2 \times 10^{-6} \text{ ppbv m}^{-1}$ ). The inclusion of upwind transport of  $\text{NO}_2$  by advection [in 2015](#) is explored further in the main simulations below (Sect. 2.3).

280

## 285 Chemistry

FORCAsT v2 incorporates 576 chemical reactions involving 411 species. As in Wei et al. (2021), our simulations use the Caltech Atmospheric Chemistry Mechanism 3 (CACM3) with the Reduced Caltech Isoprene Mechanism (RCIM; Wennberg et al., 2018) to describe isoprene oxidation under low-NO<sub>x</sub> conditions. Simple sesquiterpene chemistry is represented using β-caryophyllene oxidation by O<sub>3</sub>, OH and NO<sub>3</sub> as a proxy for all sesquiterpenes (Table S2), with reactivity dominated by O<sub>3</sub>.

290 These reactions form a number of oxidation products including various peroxy radicals, HCHO, lumped organic acids, ketones and aldehydes, which continue to react with oxidants, NO, HO<sub>2</sub> and, in some cases, undergo UV photolysis (Wei et al., 2021). However, the reactivity and product formation from sesquiterpenes is highly uncertain due to lack of measurements. All gas species concentrations are calculated prognostically. O<sub>3</sub> concentrations (mol mol<sup>-1</sup>) are initialised at heights *z* based on observations up to 79 m and extrapolated and bounded by a maximum concentration of 50 ppbv above 2000m as in the  
295 following:

$$\begin{aligned} 2.0 \times 10^{-9} + (z \times 0.15 \times 10^{-9}): z \leq 37\text{m} \\ 10 \times 10^{-9} + (z \times 0.03 \times 10^{-9}): 37\text{m} < z \leq 2000\text{m}. \quad (\text{Eq. 12}) \\ 50 \times 10^{-9}: 2000\text{m} < z \end{aligned}$$

We initiate the simulation at midnight UTC, 20:00 local time; at this time most trace gas concentrations are low and do not  
300 need to be initialised.

### Transport and fluxes

The mass flux for gas-phase species is described by Eq. 13:

$$\frac{\partial c}{\partial t} = \frac{\partial}{\partial z} \left( K \frac{\partial c}{\partial z} \right) + S_c \quad (\text{Eq. 13})$$

305 where *c* is the mixing ratio of a chemical species, *S<sub>c</sub>* represents the sum of emissions, deposition, and advection tendencies at each layer (s<sup>-1</sup>), and *K* is the eddy diffusivity coefficient (m<sup>2</sup> s<sup>-1</sup>).

Emissions, deposition and advection contributions are summed for each layer to calculate the rate of change (*S<sub>c</sub>*) at each layer and are passed to the vertical transport solver. Numerically, these tendencies are incorporated through operator splitting: the term *S<sub>c</sub>Δt* is added to the right-hand side before the implicit vertical transport solve. The chemical solver is applied subsequently. This operator splitting is described and evaluated in Wei et al. (2021).

310 In this version, we move soil NO emissions from being a lower boundary condition to an emission contributing to *S<sub>c</sub>* in the lowest atmosphere layer. Surface emissions and deposition are therefore treated explicitly within the chemical source terms prior to the transport step. To ensure that turbulent transport redistributes species within the column without introducing additional sources or sinks at the domain boundaries, the transport solver applies zero-flux (Neumann) boundary conditions at both the lower and upper boundaries. At each timestep, new concentrations of all chemical species are calculated at each level  
315 using an implicit method to solve the partial differential equations required in calculation of mixing. The zero-flux upper boundary means there is no representation of entrainment but O<sub>3</sub> concentrations in our simulations equilibrate within a day to 20 ppb at 1 km and 50 ppb at 3 km and remain stable. As this is the first time the model has been used to simulate a longer

Deleted: to

Deleted: give

Deleted: +C

Deleted: concentration or

Deleted:

Formatted: Subscript

Deleted: *C* is net chemical production (s<sup>-1</sup>),

Deleted: mass injection

Formatted: Font: Italic

Formatted: Font: Italic, Subscript

Deleted: mass injected

Deleted: to

Formatted: Font: Italic

Formatted: Font: Italic, Subscript

Deleted: now

time period without nudging (Otu-Larbi et al., 2021), improvement of the upper boundary concentrations should be considered in future.

330 Temperature is initialised below the canopy using a linear fit between the measured ground and canopy height temperatures. Above the canopy, initial temperature is extrapolated from the canopy level measurement using a prescribed lapse rate. Fluxes of heat at each layer are as follows:

$$\frac{\partial T}{\partial t} = \frac{\partial}{\partial z} \left( K \frac{\partial T}{\partial z} \right) + S_h \quad (\text{Eq. 14})$$

335  $S_h$  represents sources and sinks of heat ( $\text{K s}^{-1}$ ), such as from vegetation. Equation 14 is solved at each model layer to give prognostic temperature using surface soil temperature in the formation of the lower-level boundary condition.

The value of  $K$  used to describe both heat and mass transport is computed at each level, with separate equations for the surface layer, the boundary layer and the free atmosphere.  $K$ -theory is a first-order closure theory that assumes that turbulent flow leads to transfer down a concentration gradient (Raupach, 1989), where  $K$  dictates the efficiency of turbulent mixing based on

340 atmospheric stability. The equations for the above-canopy profile of  $K$  are described in the SI and in Wei et al. (2021).

Below the canopy,  $K$  is a function of  $\sigma_w$  at height  $z$ :

$$K = Tl \times \sigma_{w(z)}^2 \times R \quad (\text{Eq. 15})$$

$Tl$  is a scaling factor with units of length:

$$Tl = \frac{0.3 \times h}{u_*} \quad (\text{Eq. 16})$$

345 Raupach et al. (1989) suggests scaling by an  $R$  factor within the canopy to account for near-field effects, which describes changes to conditions close to an emissions source or boundary, especially from a non-uniform source:

$$R = \frac{1 - e^{-\frac{\tau}{Tl}} \times (\tau - Tl)^{3/2}}{(\tau - Tl \times e^{-\frac{\tau}{Tl}})^{3/2}} \quad (\text{Eq. 17})$$

The  $R$  factor describes the reduction of  $K$  within the canopy explicitly. However,  $\tau$  is undefined and must be estimated. We perform 3-day sensitivity studies to select  $\tau/Tl = 1.6$  and evaluate the effect on concentration profiles of  $\text{O}_3$  and isoprene (Fig.

350 S8, S9).

$K$  is first calculated above the canopy using observed  $\sigma_w$  at 55 m (Sect. 2.1). The in-canopy  $K$  values are derived at each model level using a function that modifies the observed  $\sigma_w$  to decrease with height  $z$  (a result of surface friction and interception by the canopy). For the ATTO site, we adapt the function for  $\sigma_{w(z)}$  within the canopy from Wei et al. (2021), which uses observations at two heights (above and within the canopy) and interpolates linearly at heights in between. As the ATTO site 355 has limited measurements within the canopy, it is advantageous to describe the in-canopy mixing using only above canopy measurements. To achieve this, we calculate the variation in  $\sigma_{w(z)}$  with height within the canopy as in Raupach et al. (1989) (Eq. 18), changing the relationship from a linear to a sine-based function. This results in a faster reduction in mixing with height, reflecting a greater separation between the canopy and above-canopy in the tropical forest. With this adjustment,

measured in-canopy  $\sigma_{w(24)}$  is reproduced from above-canopy  $\sigma_w$ , giving confidence in our estimation at other heights (Fig. S10). This implies that the vertical mixing can be described using only above-canopy observations, and therefore simulations can be performed during periods when in-canopy measurements are missing. For height  $z$  below canopy height, wind deviation  $\sigma_{w(z)}$  is calculated from  $\sigma_{w(55)}$  at 55m:

$$\sigma_{w(z)} = 0.5 \times \sigma_{w(55)} + 0.45 \times \sigma_{w(55)} \times \cos\left(\pi \times \left(1 - \frac{z}{55}\right)\right) \quad (\text{Eq. 18})$$

Between the canopy height and 55 m,  $K$  is smoothed to transition to above canopy values of  $K$  (see Supplementary model description) without discontinuity. Figs. S1 and S2 show  $\sigma_{w(55)}$  and  $u_*$  used to produce  $K$  below the canopy.

### 2.3. Simulations

Using the parameters above, we produce five simulations of the ATTO site for the periods 1–13 November 2013 and 11–23 November 2015 to explore effects of meteorology, sesquiterpenes and upwind transport of  $\text{NO}_2$  in more detail (Table 2). The model uses observations of wind direction,  $\sigma_w$ ,  $u_*$  and PAR recorded above the canopy (55 m) as described in Sect. 2.1. (Figs. S1, S2). For simulations of 2013, we duplicate  $\sigma_w$  from 2015 due to missing observations, assuming that the average turbulence was similar between years. [ATTO observations of turbulence regimes show variability across seasons and years \(Botía et al., 2020; Cava et al., 2022; Mortarini et al., 2022\)](#), but there are no direct comparisons of how  $\sigma_w$  changes from one year to the next. November 2013 is considered to represent an average November, whereas the 2015 period is used for comparison to an El Niño period in which increased biomass burning occurred. [Biomass burning advection is not considered in 2013 as there was limited fire activity during November.](#)

Simulation name	$\text{NO}_x$ source	Sesquiterpene emission
<b>2013</b>	Soil NO	Yes
<b>2013 No SQT</b>	Soil NO	No
<b>2015</b>	Soil NO, transport of $\text{NO}_2$	Yes
<b>2015 No SQT</b>	Soil NO, transport of $\text{NO}_2$	No
<b>2015 pristine</b>	Soil NO	Yes

**Table 2: Variables in five simulations investigating effects of  $\text{NO}_x$  sources and sesquiterpene emissions.**

We test the hypothesis that sesquiterpene emissions have an important role in canopy-scale  $\text{O}_3$  deposition fluxes via chemical removal inside the canopy by including simulations with and without sesquiterpene emissions. We also consider if transported  $\text{NO}_2$  from biomass burning in 2015 could impact  $\text{O}_3$ , BVOC and  $\text{NO}_x$  exchange at the canopy top.

## 2.4. Canopy exchange calculations

To estimate a canopy exchange flux of NO<sub>x</sub> and O<sub>3</sub> ( $E_x$ ; nmol m<sup>-2</sup> s<sup>-1</sup>) from the canopy to the atmosphere, we use the formula defined in Rummel et al. (2007), which specifically accounts for temporary storage of trace gases within the canopy:

$$E_x = \int_0^h Chem_{net}(z)dz - \int_0^h Dep(z)dz + \int_0^h Emission(z)dz + \frac{d}{dt} \int_0^h [x](z)dz \quad (Eq. 19)$$

385 Where  $x$  is either O<sub>3</sub> or NO<sub>x</sub> and each term describes the integrated sum of chemistry, deposition, emission rates and storage across the vertical canopy levels  $z$  from soil level to canopy height  $h$ .  $Chem_{net}(z)$  refers to the net chemical production and loss rates at each height  $z$ . The storage term  $\frac{d}{dt} \int_0^h [x](z)dz$  represents any gas that is formed within the canopy or otherwise trapped within the canopy, that causes the in-canopy concentration to change. For example, soil-emitted NO does not immediately become an above-canopy flux, for a time it is trapped within the canopy and can be identified by an increase in  
390 within-canopy NO<sub>x</sub> concentrations.

In the case of NO<sub>x</sub> in 2015, it is useful to further separate the canopy exchange into the contributions from transported NO<sub>2</sub> and soil NO to calculate a canopy escape efficiency of soil NO<sub>x</sub>. The contribution from upwind NO<sub>2</sub> transport into the canopy,  $E_{NOx\_transp}$ , is estimated as the canopy exchange from a simulation of 2015 with no soil NO. This contribution is removed from simulations that contain both soil NO and transported NO<sub>2</sub> to give the soil NO<sub>x</sub> escape efficiency.

395 
$$Escape_{NOx} = E_{NOx} - E_{NOx\_transp} \quad (Eq. 20)$$

## 3. Results

### 3.1. Simulation Evaluation

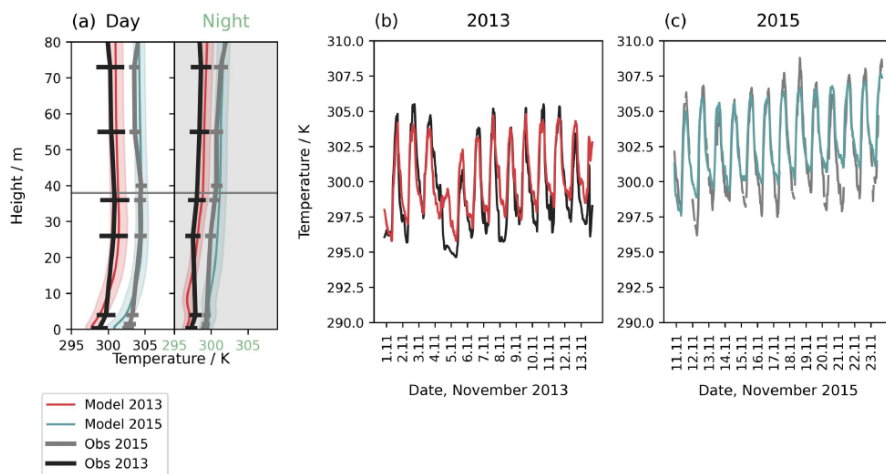
November 2013 at the ATTO site was a typical month in terms of temperature and wind velocity (Schmitt et al., 2023). November 2015 was atypical; El Niño conditions caused temperatures at ATTO to be 3 °C higher compared to 2013 and 1.5  
400 °C higher across the Amazon compared to average (Jiménez-Muñoz et al., 2016). The 2015/16 El Niño drought reached maximum intensity in October 2015, with forest fires in November continuing to burn as though it was still the dry season (Ribeiro Neto et al., 2022; Silva Junior et al., 2019). During this period, the wind at ATTO predominantly originated from the Arc of Deforestation in the East (Fig. S11a), the location of enhanced fire activity (Silva Junior et al., 2019).

Measurements of atmospheric composition at ATTO during November 2015 showed increased OH reactivity, monoterpene  
405 emissions and oxidation product-to-isoprene ratios compared to previous years (Pfannerstill et al., 2018, 2021; Yáñez-Serrano et al., 2015, 2018). Daily mean O<sub>3</sub> concentrations in November 2015 were elevated compared to previous years, reaching up to 28 ppbv at 38 m, whereas 2013 concentrations varied between 4 and 16 ppbv at the canopy top, typical for the ATTO site (Fig 11b).

We evaluate temperature and wind in our simulations and find the model reproduces temperatures in the 2013 and 2015 periods  
410 well ( $r^2=0.80$ ), albeit with a smaller diurnal range than observed and a stronger vertical gradient below the canopy (Fig. 2). Previous applications of the FORCAst model also find the simulated diurnal variability is lower than observed (Wei et al.,

2021). The model captures the difference between years and the day-to-day variability (Figs. 2b, 2c). The surface-level temperatures, which affect the soil NO emissions, reproduce night-time observations but underestimate the maximum temperatures in the daytime. The horizontal wind profile and hourly variability within the canopy is reproduced (Fig. S12).  
415 Above the canopy, however, the nighttime wind speed is underestimated on several nights, especially in 2013. Measurements show windspeeds above the canopy are frequently maintained around 2–4 m s<sup>-1</sup> overnight at 70 m, whereas friction velocity, which controls simulated wind speed, drops substantially, driving this underestimation (Fig. S12b).  
Divergence between friction velocity and horizontal wind speed above the canopy has implications on vertical mixing within the model. Observed wind speeds are low in the canopy at night, but remain high above the canopy. This indicates decoupling  
420 between the canopy and above under stable, stratified nighttime conditions. Frequently in 2013 and on several nights in 2015, nights show high wind shear and sustained wind speeds above the canopy (Fig. S13). Richardson numbers in both periods are above 0.25 at night, which suggests turbulence is suppressed and intermittent (Fig. S14). However, the model likely overestimates the degree of turbulence suppression in 2013. The simulated flow has very low shear at night, meaning shear-driven mixing in the boundary layer is underestimated (Fig. S13a, S14c). This arises from the model reliance on friction  
425 velocity to constrain turbulent exchange, meaning intermittent turbulence is not captured when friction velocity is low. As a result, vertical mixing in the above-canopy space is overly weak on some nights in the simulations, with possible implications for the representation of exchange with the canopy.  
Below the canopy, vertical turbulent exchange in our simulations shows strongly decreased vertical mixing at night, with stable air throughout the canopy especially between 1:00–5:00 local time (5:00–9:00 UTC) in both years. By midday, the canopy is  
430 well-mixed down to the lowest 20%–30%, which remains more separated from the air above (Fig. S15). Mixing below the canopy is enhanced in the 2015 period compared to the 2013 period during daytime on average across the simulation periods (Fig. S16). In observations, Pfannerstill et al. (2018) also found increased turbulent features during 2015, [however we also note that missing observations of 2013  \$\sigma\_w\$  may affect our results](#). We find the meteorological performance of the model at this site to be comparable to simulations of the temperate forest, even when extending the simulation time considerably from  
435 previous 2-day studies (Wei et al., 2021).  
As a final evaluation of the model, we consider the partitioning of energy into latent and sensible heat fluxes above the canopy (Fig. S17). Average maximum hourly latent heat fluxes are 250 W m<sup>-2</sup> for the 2013 simulation period and 310 W m<sup>-2</sup> for the 2015 period, in good agreement with observations from the nearby LBA-k34 flux tower, which recorded hourly maxima of 250 and 300 W m<sup>-2</sup> for wet and dry season means, respectively (Gerken et al., 2018). Sensible heat fluxes are 80 W m<sup>-2</sup> and  
440 100 W m<sup>-2</sup> in 2013 and 2015, respectively, compared to 110–150 W m<sup>-2</sup> in the nearby observations for wet and dry seasons. As a result of the lower magnitude and differences in the sensible heat flux diurnal cycle compared to observations, the Bowen ratio is higher in the morning and lower in the evening relative to the flux site values. However, the mean values of 0.4 in 2013 and 0.32 in 2015 (Fig. S17c) are close to observations (0.5) and represent an improvement over many land surface models (Restrepo-Coupe et al., 2021). These values suggest 2015 was not strongly water-limited in our simulations, with energy  
445 partitioning primarily responding to radiation. Observations of pristine tropical forests typically show seasonal cycles driven

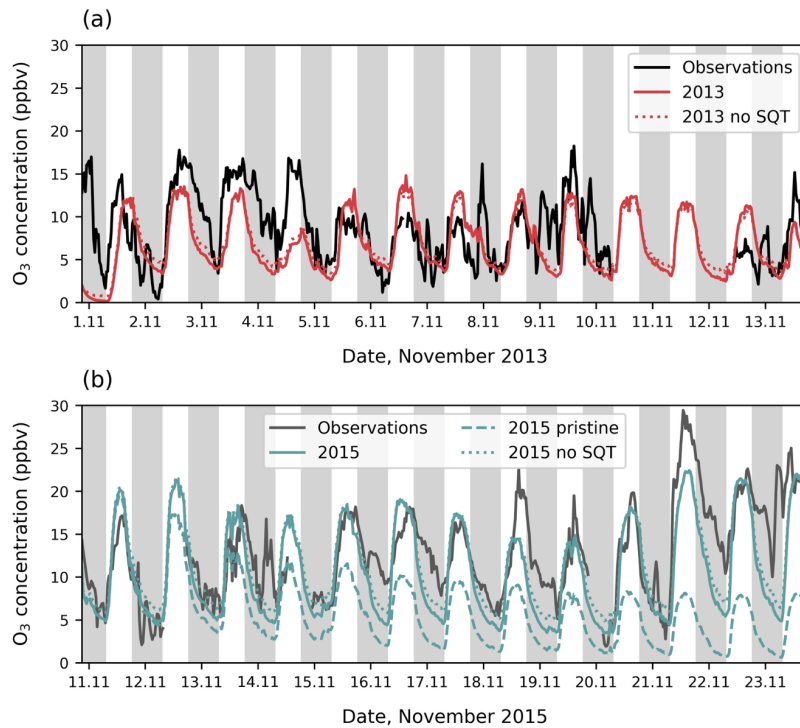
by radiation, with water stress rarely limiting (Restrepo-Coupe et al., 2021), making the model behaviour plausible, despite lacking directly comparable observations.



450 **Figure 2: (a) Mean vertical profile of air temperature for day and night for simulations of November 2013 (red solid line), 2015 (teal solid line) and observations in 2013 (black solid line) and 2015 (grey solid line). Horizontal lines and shading show the daily mean standard deviation. (b) and (c) show the time series evaluation at 36 m for (b) 2013 and (c) 2015 simulation periods.**

Figure 3a shows the model can reproduce the general magnitude and diurnal cycle of  $O_3$  concentrations in the 2013 period. However, day-to-day variability is not well captured, especially the patterns in peak  $O_3$  concentrations among different days. 455 One of the vertical mixing components ( $\sigma_w$ ) is not available for 2013, so any contribution to day-to-day variability that may occur from mixing cannot be fully represented. In November 2015, the magnitude of measured  $O_3$  concentrations can only be reproduced when upwind transport of  $NO_2$  from fires is included (Fig. 3b). Without transported  $NO_2$ ,  $O_3$  concentrations in the 2015 period are lower than 2013 concentrations despite higher temperatures, but when included, average  $O_3$  concentrations over the 2015 simulation period are almost doubled. We find that inclusion of transported  $NO_2$  captures the daily variability 460 in peak  $O_3$  concentrations on most days (Fig. 3b). This suggests that advected biomass burning air masses, resulting from higher fire activity in November 2015 compared to average (Ribeiro Neto et al., 2022; Silva Junior et al., 2019), are the main driver of higher  $O_3$  concentrations at the site in 2015 rather than other meteorological differences such as higher temperature. Sensitivity tests in which sesquiterpene emissions are switched off are 1–2 ppbv higher at night, providing a better match to observations on average but not necessarily capturing the day-to-day variability better (Figs. 3, 4a, 4b). Since we use a high

465 O<sub>3</sub> reactivity to represent sesquiterpenes, the comparison of simulations with and without sesquiterpenes gives an uncertainty  
range on the effect of these emissions on O<sub>3</sub> concentration.



470 **Figure 3:** Above-canopy O<sub>3</sub> concentrations at 38 m from observations (solid black line) compared to simulations (coloured lines) for  
470 (a) November 2013 and (b) November 2015. Axis ticks are placed at midnight, and grey shading shows nighttime. In (a) simulations  
include O<sub>3</sub> concentrations with (red solid line) and without sesquiterpene emissions (red dotted line). In (b) simulations include O<sub>3</sub>  
concentrations when transport of NO<sub>2</sub> is included (teal solid line), without transported NO<sub>2</sub> (teal dashed line) and without  
sesquiterpene emissions (teal dotted line).

475 In both 2013 and 2015 simulation periods, the model performs worst overnight, often failing to capture nights in which O<sub>3</sub> is  
maintained at high concentrations, including in the lower canopy on three nights in 2015 (Fig. 3). High nighttime O<sub>3</sub> is

on November 14<sup>th</sup> 2015, are most likely related to missing turbulent features in our model. Nights with high O<sub>3</sub> concentrations above the canopy are often associated with high wind shear that is not reproduced by the model, suggesting turbulence within the boundary layer that brings O<sub>3</sub> to the canopy top (Fig. S13). Below the canopy, nighttime O<sub>3</sub> concentrations are reproduced on most nights in the model. The model captures the O<sub>3</sub> diurnal cycle more closely in the tropics compared to previously simulated temperate forests (Ashworth et al., 2015; Wei et al., 2021) due to the smaller influence from transported air masses at this site.

Figures 4a and 4b confirm that, whilst the daytime O<sub>3</sub> profiles are a good match to observations, nighttime profiles are underestimated, especially above the canopy. The step-change in O<sub>3</sub> gradient below the canopy in observations of the 2013 period suggests some decoupling between the canopy and above occurs, as also indicated by the sustained wind and low friction velocity above the canopy, described above (Figs. S12b, S12c). The lack of intermittent turbulence above the canopy in the simulations leads to underestimation of the above canopy O<sub>3</sub> profile, but decoupling results in a smaller bias below the canopy. The shape of the daytime vertical profile in the 2015 period is better captured than in the 2013 period; the observed 2013 vertical concentration gradient is steeper than 2015 but this is not replicated by the model.

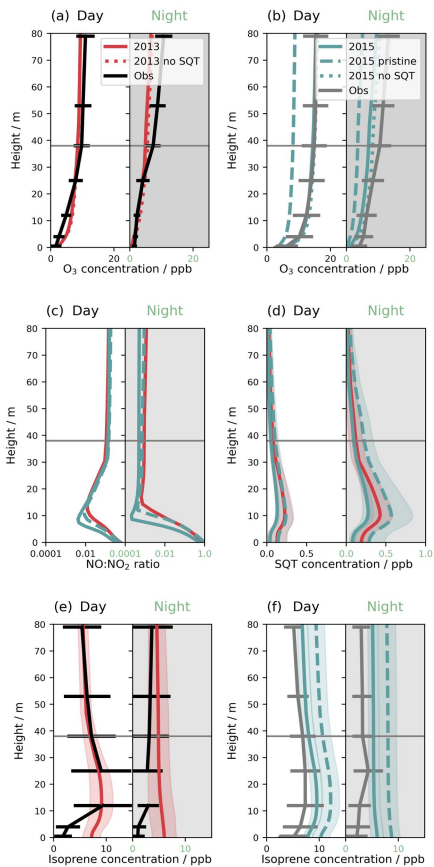
Simulations of 2015 with transported NO<sub>2</sub>, which produces additional O<sub>3</sub>, consequently have a higher oxidative capacity. In pristine conditions, midday peak OH concentrations above the canopy are on average  $1.3 \times 10^6 \text{ cm}^{-3}$ , decreasing to  $0.4 \times 10^6 \text{ cm}^{-3}$  within the canopy (not shown). The addition of transported NO<sub>2</sub> increases OH by 2x above the canopy, with diminishing differences between simulations below the canopy. Literature values from recent site measurements report  $1 \times 10^6 \text{ cm}^{-3}$  (Jeong et al., 2021), of similar magnitude to our simulations.

Transported NO<sub>2</sub> is also associated with a change in the NO:NO<sub>2</sub> ratio (Fig. 4c) in the lower canopy. In pristine conditions, the NO:NO<sub>2</sub> ratio is 0.5 and 1 at the soil surface in the day and night, respectively, decreasing to 0.35 (day) and 0.5 (night) when NO<sub>2</sub> transport is included in the 2015 simulation period. The elevated O<sub>3</sub> concentrations expedite the cycling of NO to NO<sub>2</sub>, which removes NO in the dark lower canopy. By 10 m height within the canopy, NO concentrations are near zero in all simulations; NO is only re-formed closer to the canopy top where daytime photolysis is possible. Transported NO<sub>2</sub>, of which very little reaches the soil level, does not strongly affect the NO:NO<sub>2</sub> ratio and the above-canopy ratio does not depend strongly on the simulation.

Even with the inclusion of transported NO<sub>2</sub>, NO<sub>x</sub> concentrations above the canopy remain below 1 ppbv (Fig. S18). Transported NO<sub>2</sub> can increase the above-canopy nighttime NO<sub>2</sub> concentrations from ~300 pptv to up to 600 pptv (e.g., on the 16<sup>th</sup> November 2015), increasing daytime NO as well. The values in pristine conditions compare well to observations at another Amazon site that measures pristine nighttime values of 350 pptv but find pollution enhancements of up to 1800 pptv (Cordova et al., 2004). Simulations show a distinct NO peak at sunrise as soil emissions are released from the canopy. These peaks show significant daily variability from 25 pptv to over 100 pptv, with daytime mean concentrations of 25 pptv without transported NO<sub>2</sub> and 50 pptv when NO<sub>2</sub> transport is included (Fig. S18e). The addition of transported NO<sub>2</sub> results in a less steep decay in NO from the midday peak. These values fit with observations recording 20 pptv – 50 pptv above the Amazon forest canopy (Bakwin et al.,

1990; Kuhn et al., 2010). Soil NO emissions therefore affect above-canopy NO<sub>x</sub> concentrations significantly across all simulations.

515 Ground-level concentrations of NO depend strongly on O<sub>3</sub> concentrations, with even a few ppbv of O<sub>3</sub> rapidly removing emitted NO. Our simulations show very low nighttime O<sub>3</sub> concentrations (in agreement with observations), resulting in NO concentrations of 2 pptv – 4 ppbv. This is consistent with observations from Rummel et al. (2002) who record lower NO concentrations of up to 2 ppbv but higher nighttime O<sub>3</sub> values. Conversely, ground-level daytime O<sub>3</sub> at the ATTO site is higher than measured by Rummel et al. (2002) and simulated daytime NO concentrations are below their measurements of 1.2 ppbv. Our daytime ground-level NO concentrations are closer to those of Bakwin et al. (1990) at 450 pptv.

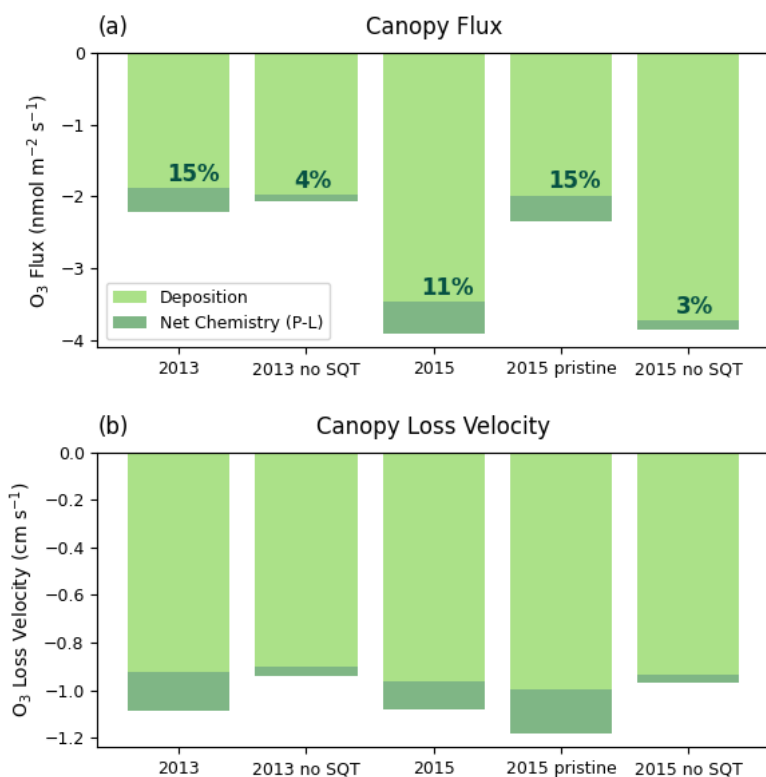


520 **Figure 4:** Mean vertical profiles for day and night in simulation periods of 2013 (red solid line), 2015, including transported  $\text{NO}_2$  (teal solid line) and 2015 without transported  $\text{NO}_2$  (teal dashed line) for (a)  $\text{O}_3$  in 2013, (b)  $\text{O}_3$  in 2015, (c)  $\text{NO}:\text{NO}_2$  ratio, (d) sesquiterpene concentrations, (e) isoprene concentration in 2013 and (f) isoprene concentration, in 2015. Simulations are compared to observations (a) of  $\text{O}_3$  in November 2013 (black solid line), (b) of  $\text{O}_3$  in and November 2015 (grey solid line), (e) of isoprene in 525 November 2012 (black solid line) and (f) of isoprene in October 2015 (grey solid line). Error bars and shading show one standard deviation of daily means. The grey horizontal line indicates the canopy height.

530 High temperatures and PAR in the 2015 simulation increase BVOC emission compared to the 2013 simulation; isoprene emissions increase by 50% and sesquiterpenes by 35% (Fig. S19). However, the concentration profiles (Figs. 4d–4f) are also related to background chemical composition. Simulations of the 2015 period in pristine conditions have higher BVOC concentrations compared to those with transported NO<sub>2</sub>, as the lower oxidative capacity in pristine conditions leads to slower oxidation. With NO<sub>2</sub> transport included in 2015, isoprene concentrations are similar to the 2013 period concentrations, in both simulations and observations. The higher emissions in the 2015 period are balanced by increased oxidation. Concentrations of sesquiterpenes are lowest in 2015; the increased loss from the higher O<sub>3</sub> concentrations outweighs the increase in emissions (Fig. 4d). In all simulations, sesquiterpenes build up overnight within the canopy as vertical mixing declines and oxidation decreases, leading to higher concentrations at night compared to during the day in agreement with observations (Jardine et al., 2011).  
Very low isoprene concentrations are recorded below the canopy (Fig. 4e, 4f) that are consistently overestimated by the model. Some studies find isoprene loss fluxes to tropical soils (e.g., Pugliese et al., 2023) that are not explored in this study.

### 540 3.2. O<sub>3</sub> losses in the canopy

Figure 5a shows the mean total canopy flux of O<sub>3</sub> over the simulation period, divided into net chemical loss and deposition (as in Eq. 19). The O<sub>3</sub> mostly originates from above the canopy, meaning the canopy is a net O<sub>3</sub> sink. The total flux in 2013 is -2.4 nmol m<sup>-2</sup> s<sup>-1</sup> compared to -3.9 nmol m<sup>-2</sup> s<sup>-1</sup> in 2015, whereas the total flux in the 2013 simulation period and an idealised 2015 period with no transported NO<sub>x</sub> are very similar (i.e., the main difference between 2013 and 2015 simulation periods is related to effects of transported NO<sub>x</sub>). Simulations without sesquiterpene emissions have very little effect on the total flux.  
545 Considering the breakdown of the flux into chemical and depositional components, we find that deposition accounts for the majority of O<sub>3</sub> losses in all simulations. The fraction of total loss that is due to chemistry is slightly higher in simulations without transported NO<sub>2</sub> at 15% compared to 11% when transport of NO<sub>2</sub> is included (Fig. 5a). Without sesquiterpenes, the fraction of O<sub>3</sub> loss due to chemistry reduces to 3%–4%, however the decrease in chemical flux is partly compensated by an increase in deposition flux. This may suggest that sesquiterpenes can reduce the deposition flux to vegetation through reducing the O<sub>3</sub> available for deposition and thus have the potential to reduce O<sub>3</sub> damage to vegetation. On the other hand, since the difference in the total flux is small, it indicates that the total O<sub>3</sub> in-canopy loss is somewhat resistant to uncertainties in sesquiterpene emissions and chemistry.  
550



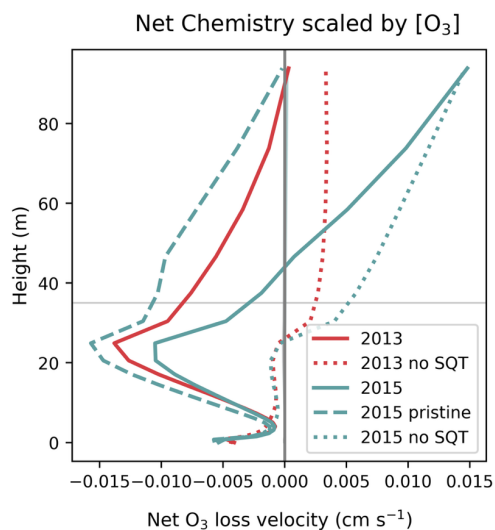
555

**Figure 5: (a) The mean flux of O<sub>3</sub> in nmol m<sup>-2</sup> s<sup>-1</sup> and (b) the canopy-scale deposition velocity in cm s<sup>-1</sup> divided into deposition (light green) and net chemistry (dark green). Text given in (a) indicates the percentage of the total flux that is chemical destruction.**

560 Figure 5b shows the equivalent losses presented as a canopy-scale deposition velocity. Variability in the canopy deposition velocity is much smaller than in the total O<sub>3</sub> flux, with a range of -0.9 to -1.2 cm s<sup>-1</sup> among the simulations, implying that most of the difference in flux is related to differences in the O<sub>3</sub> concentrations. The major differences are (1) a small variability of -0.04 cm s<sup>-1</sup> in deposition velocity between simulations, (2) an increase in chemical loss velocity in the absence of transported NO<sub>2</sub> in 2015, and (3) a decrease in chemical loss velocity without sesquiterpene chemistry.

Diurnal patterns of individual flux terms (chemistry, deposition and storage) show the same features identified by Rummel et al. (2007) such as an increase in storage in the morning as vertical transport brings O<sub>3</sub> into the canopy from above (Fig. S20). Observed fluxes are also similar in magnitude to our simulations but cannot be directly compared as they depend strongly on O<sub>3</sub> concentration. Observations of canopy deposition velocities are larger in the wet season compared to the dry season, attributed to humidity-driven stomatal limitation in the dry season. Our simulated deposition velocities are within the range of wet season observations but are higher than dry season averages of ~0.5 cm s<sup>-1</sup> (Rummel et al., 2007). Our simulations show high relative humidity (Fig. S21) and daytime temperatures (Fig. 2) close to the simulation optimum parameter for stomatal conductance (301 K), suggesting little stomatal limitation and therefore ‘wet season’ behaviour. This is consistent with evaluation of the energy balance and Bowen ratio described above (Sect. 3.1, Fig. S17). Day-to-day variability in deposition velocity in the simulations follows variability in temperature and PAR (Fig. S22). The 2013 period exhibits lower average PAR and greater daily variability (including a cool, cloudy day on the 4<sup>th</sup>), resulting in lower average stomatal conductance than the 2015 period (Fig. S23). However, differences in deposition velocity between simulations are likely also related to changes in O<sub>3</sub> distribution within the canopy.

In the remainder of this section, we consider the chemistry within the canopy, first using Fig. 6 to explore differences in chemical loss velocity between years and simulations. The vertical profiles of net chemistry in Fig. 6 elucidate the role of BVOCs and soil NO in driving O<sub>3</sub> losses within the canopy. In addition to removal by BVOCs in the canopy, soil NO is responsible for O<sub>3</sub> removal at the lowest model level, which compares to the reports from another Amazonian site (Gut et al., 2002). The chemical loss velocity profiles for simulations without sesquiterpene emissions show that loss by reaction with soil NO is of similar magnitude to O<sub>3</sub> removal by other BVOCs and the in-canopy profiles are very similar between years, which suggests sesquiterpenes are responsible for the differences in net chemistry. We find that consideration of both sesquiterpene emissions and O<sub>3</sub> concentrations are required to explain the canopy average loss velocity; there is a robust but non-linear relationship between canopy O<sub>3</sub> chemical loss and the ratio of sesquiterpene emissions to O<sub>3</sub> concentrations at 30 min resolution (Fig. S24). A decrease in chemical loss in 2015 in polluted conditions can be explained by an increase in O<sub>3</sub> concentrations, and faster losses in 2015 in pristine conditions can be explained by an increase in sesquiterpene emissions compared to 2013, on account of higher PAR and temperature. Differences between simulations are greatest at 20–25 m where the leaf area density (and associated BVOC emissions) is highest, whereas at the soil surface, chemical loss frequencies are similar.



595 **Figure 6:** Vertical profiles of simulated net O<sub>3</sub> chemistry (production – loss) divided by O<sub>3</sub> concentration to give the loss velocity per molecule for simulation periods in 2013 (red lines) and 2015 (teal lines). Sensitivity tests show simulations without sesquiterpenes (dotted lines) and 2015 without transport of NO<sub>2</sub> (teal dashed line). The horizontal line indicates the canopy top height.

Figure 7 shows the diurnal cycle of chemical production and loss occurring at 25 m, to demonstrate how chemistry varies over the day at the bulk canopy height (Fig. 1). Considering the individual reactions involved in O<sub>3</sub> chemical loss (Fig. 7, green shading), sesquiterpene ozonolysis dominates at all times of day and is entirely responsible for nighttime chemistry at this height. Other BVOCs contribute to O<sub>3</sub> destruction during the afternoon and 2015 has a more substantial morning contribution from radical losses. Considering the whole canopy, over the diurnal cycle, chemistry is most important during the night, where it can account for 40% the total O<sub>3</sub> losses (Fig. S20). During the day, its contribution to the canopy O<sub>3</sub> flux diminishes to 5%, which is in response to an 8-fold increase in deposition flux as stomatal pathways become available, rather than a significant change in chemistry.

605

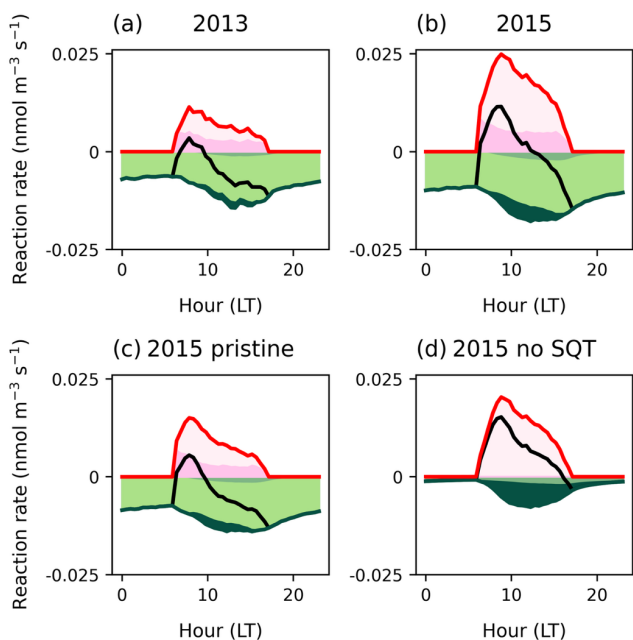
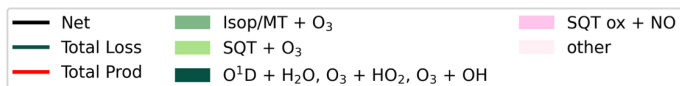


Figure 7: Mean diurnal cycles at 25 m of chemical reactions for O<sub>3</sub> loss (green solid line), production (red solid line) and net chemistry (black solid line). Individual reactions are shaded showing sesquiterpene ozonolysis (light green shading), isoprene / monoterpenes + O<sub>3</sub> (medium green shading) and inorganic O<sub>3</sub> loss (dark green shading). For O<sub>3</sub> production reactions, β-carophyllene oxidation products is the largest uncertainty (dark pink shading).  
610

The diurnal cycle reveals that even at 25 m, simulations switch to net O<sub>3</sub> production after sunrise and the breakdown of the nighttime boundary layer (approx. 6am) (Fig. 7, black solid line). O<sub>3</sub> production (Fig. 7, red solid line) is driven by a large number of oxidation products in the presence of NO; the three largest contributors are isoprene oxidation products, HO<sub>2</sub> and sesquiterpene oxidation products. As the largest uncertainty, the contribution from sesquiterpene oxidation products is shown in dark pink shading; it counteracts a substantial portion of daytime losses due to sesquiterpenes at this height. Production is smallest in 2013 and enhanced in the presence of transported NO<sub>x</sub> (Fig. 7b) such that net production of O<sub>3</sub> continues until  
615

13:00 on average compared to until 10:00 in pristine conditions (Fig. 7c). Without sesquiterpenes, net O<sub>3</sub> production occurs throughout daylight hours (Fig. 7d). The significant diurnal variability in O<sub>3</sub> production suggests that canopy escape efficiencies of precursors (especially NO<sub>x</sub> and sesquiterpenes) should be investigated across the diurnal cycle.

In the mean vertical profile (Fig. 6), the transition to net O<sub>3</sub> production occurs at different heights among simulations. Addition of transported NO<sub>2</sub> triggers net production at 40 m whereas in pristine conditions, profiles in the 2013 and 2015 simulation periods both show net loss of O<sub>3</sub> up to 100 m. Without sesquiterpene emissions, net O<sub>3</sub> production begins immediately above the main canopy density at 25 m, where light is not strongly attenuated and can initiate photolysis (Fig. 1). Simulations with and without sesquiterpene emissions converge at around 100 m, indicating the point at which sesquiterpenes are fully oxidized. A significant portion of O<sub>3</sub> losses by sesquiterpenes occur above the canopy, implying that accurate quantification of sesquiterpene escape efficiencies is important for above-canopy chemistry.

### 3.3. The role of BVOCs in canopy chemistry

BVOC escape efficiency is controlled by their oxidation rate with respect to OH, O<sub>3</sub> and NO<sub>3</sub>, such that the faster a species can be removed (dependent on reaction rate and oxidant concentration), the lower the escape efficiency. For the oxidant concentrations at this site, escape efficiencies of primary emitted BVOCs increase in the order; sesquiterpenes << limonene < α-pinene < isoprene. Furthermore, depending on transport and oxidant concentration between simulations, BVOC escape efficiencies vary among simulations.

The escape efficiency of sesquiterpenes ranges from 45%–55% between simulations. The highest escape efficiency of 55% occurs in 2015 pristine conditions. When transport of NO<sub>2</sub> is included, this decreases to 48% as a result of higher O<sub>3</sub> concentrations. Both simulations of the 2015 period have a higher escape efficiency than the 45% in 2013. The MEGAN 2.0 BVOC emissions model includes an escape efficiency to account for BVOC losses within the canopy, based on chemical lifetime, *u*, and canopy depth (Guenther et al., 2006). This parameterisation results in canopy escape efficiencies from 10% (in the presence of high O<sub>3</sub>) to 60%. Our results, in relatively low O<sub>3</sub> conditions compared to global averages, fit realistically within this wide range. We find a significant correlation exists between daily mean escape efficiency and *u*. ( $r^2=0.69$ ,  $p<<0.05$ ; Fig. S25). This indicates that, for single-layer canopy models seeking a simple parameterisation, the current equation in MEGAN 2.0 is functional.

Isoprene and α-pinene escape efficiencies are 95% both with and without transported NO<sub>2</sub>, and in both 2013 and 2015 simulation periods. This is despite different emission magnitudes of isoprene of 4.7 and 7.3 mg m<sup>-2</sup> s<sup>-1</sup> due to varying meteorological conditions (Fig. S19). The isoprene escape efficiency of 95% with little variability is consistent with the parameterisation from MEGAN 2.0 (Guenther et al., 2006).

Conversely, limonene escape efficiency is slightly more sensitive to the environmental conditions, with escape efficiencies of 88% in pristine conditions in 2015, dropping to 84% with transported NO<sub>2</sub> and in 2013. These temperature-dependent pool emissions continue overnight when vertical mixing is slow, which allows more time for chemistry to act. This allows for

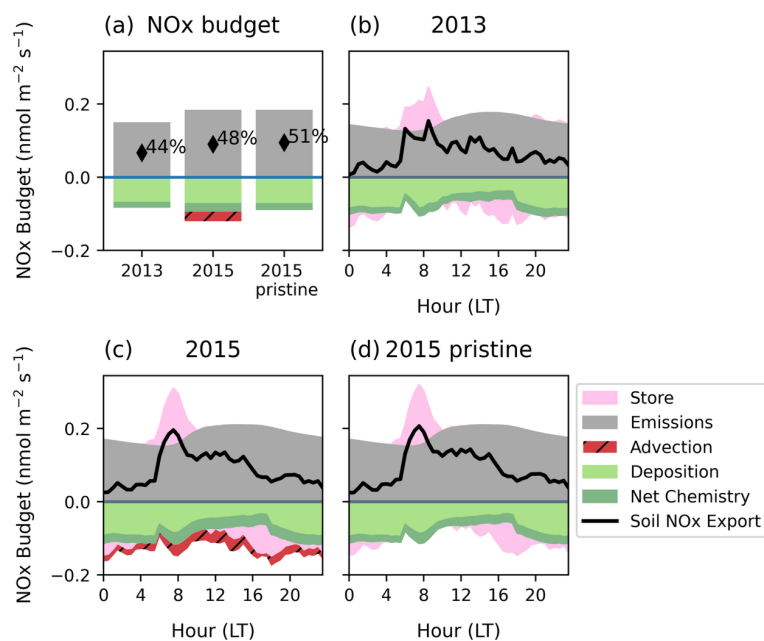
650 greater differences in escape efficiencies between simulations due to chemical environments that are overcome during the day  
when vertical mixing is highly efficient and canopy residence times are short.

### 3.4. NO<sub>x</sub> exchange with the canopy

#### 3.4.1. Soil NO<sub>x</sub> escape efficiency

655 Figure 8a shows the NO<sub>x</sub> budget terms below the canopy and the overall escape efficiency of soil NO<sub>x</sub>. The soil NO<sub>x</sub> escape  
efficiency is different than the canopy NO<sub>x</sub> flux (described in the next section) in that it excludes the contribution from upwind  
transported NO<sub>2</sub> into the canopy. To exclude this, we estimate the contribution from transported NO<sub>2</sub> entering the canopy using  
a simulation with no soil NO source and subtract this from the simulation of 2015 with transported NO<sub>2</sub> (as described in Sect.  
2.4; Eq. 20). The motivation for isolating only the soil NO that leaves the canopy is to inform how soil NO emission should  
be represented by a single-layer canopy model. The comparison between 2015 and pristine 2015 reveals changes in soil NO  
660 emission resulting from a change in chemical environment (e.g., the NO<sub>x</sub> production and loss terms depend on the background  
environment).

We find the 2013 escape efficiency of 44% is lower than the 2015 period simulations, given the consistent deposition of 0.7  
nmol m<sup>-2</sup> s<sup>-1</sup> across simulations despite lower emissions in the 2013 period. Comparing 2015 with and without transported NO<sub>2</sub>  
suggests the change in chemical environment due to upwind NO<sub>2</sub> transport has a relatively smaller effect on soil NO<sub>x</sub> escape  
665 (48% vs 51%) and therefore escape efficiency is more dependent on meteorological changes.



670 **Figure 8:** Mean diurnal NO<sub>x</sub> budget at 35 m of soil NO emissions (grey shading), transfer of upwind transported NO<sub>2</sub> into the canopy (red shading), net chemical change (dark green shading), deposition (light green shading) and storage (pink shading) within the canopy for (a) the daily mean and (b) – (c) the mean diurnal cycle in individual simulations. (a) 2013, (b) 2015 simulation periods including transported NO<sub>2</sub>; and (c) 2015 without transported NO<sub>2</sub>. In (a), the text gives the escape efficiency. In (b) – (c) The sum of all terms except upwind transported NO<sub>2</sub> (black solid line) is the soil NO escape flux.

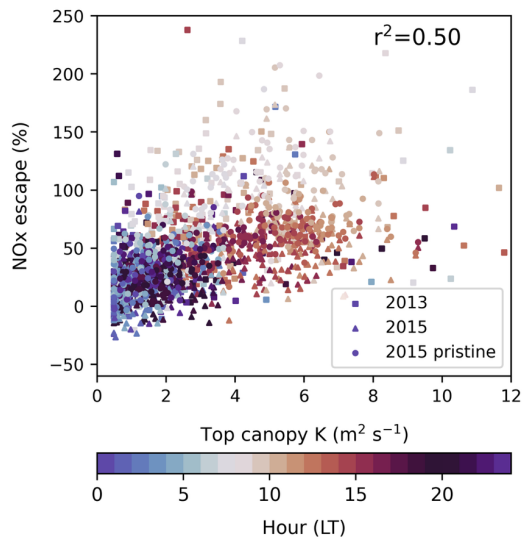
675 The diurnal cycle of soil NO<sub>x</sub> escape at the top of the canopy shows considerable variability over the day, displaying a pronounced cycle that is largely unrelated to diurnal variability in soil NO emissions (Figs. 8b–8d). Daylight hours have the highest escape efficiency, whereas NO<sub>x</sub> release overnight is suppressed by in-canopy storage and enhanced deposition fluxes. We first consider the role of storage in the diurnal pattern, which refers to NO<sub>x</sub> that becomes trapped in the canopy space due to slow vertical mixing. Our simulations find the greatest transfer of stored NO<sub>x</sub> from the canopy occurs at sunrise when stable separation between the canopy and above breaks down and photochemistry is initiated (Fig. 8, pink shading). This is very 680 pronounced in 2015 when the escape from the canopy is greater than the instantaneous soil emission rate. This indicates strong separation between the below and above-canopy environment overnight that allows NO<sub>x</sub> to build up.

NO emitted from the soil is rapidly oxidized to NO<sub>2</sub> when O<sub>3</sub> is present, but during the night, NO accumulates near the ground. At night, there is a significant flux to the soil and lower canopy surfaces (Fig. S26). As stomata are closed, this is likely non-stomatal deposition to the soil and cuticles that is high due to build-up of NO<sub>2</sub> in the lower canopy originating from the soil in low turbulence. With the onset of turbulent mixing under daylight, O<sub>3</sub> oxidises NO to NO<sub>2</sub>, which is transported upwards but partially taken up by deposition to vegetation (Breuninger et al., 2013; Chaparro-Suarez et al., 2011; Gut et al., 2002). The greatest daytime deposition flux therefore also occurs at the onset of mixing as NO<sub>x</sub> at the surface is brought to heights with greater leaf area (Fig. S26). However, the daytime deposition flux is lower than nighttime on average due to lower daytime concentrations.

685

690 Comparing across simulations, we find the escape efficiency in 2013 is lower at all times of day, with a smaller day-night contrast compared to the 2015 period (Fig. 8b). Over the course of the day, the escape efficiency varies from 25%–100% in 2013 and 30%–130% in 2015. Escape efficiencies over 100% occur when release of stored NO<sub>x</sub> in addition to emitted NO<sub>x</sub> results in canopy fluxes greater than the instantaneous emissions. On the other hand, transport of upwind NO<sub>2</sub> in 2015 does not change the mean diurnal pattern significantly (c.a. Figs. 8c, 8d); the morning storage release is slightly reduced, likely due

695



700 **Figure 9: The turbulent exchange parameter K compared to NO<sub>x</sub> escape efficiency in simulation periods of 2013 (square markers), 2015 including transported NO<sub>2</sub> (triangle markers) and 2015 without transported NO<sub>2</sub> (circle markers) in half hourly values. Shading indicated the hour in local time.**

705 Figure 9 demonstrates that vertical mixing can largely account for diurnal, daily and between-simulation variability in soil NO<sub>x</sub> escape efficiency. There is a correlation between the eddy diffusivity coefficient K and NO<sub>x</sub> escape efficiency ( $r^2=0.50$ ) across all simulations at a 30 min time resolution, suggesting half of the variability can be explained by vertical turbulence; longer canopy residence times increase the opportunity for deposition and other chemical losses in addition to in-canopy storage. Most of the variability is diurnal, although differences across days are also explained by the degree of mixing (Fig. S27). Among simulations, the reduced escape efficiency in the 2013 period relative to 2015 can be related to the slower vertical mixing, whereas the addition of transported NO<sub>2</sub> in 2015 causes an increase in net chemical removal that is unrelated to mixing parameterisations. The morning spike in NO<sub>x</sub> escape is proportionally greater than the morning increase in K (Fig. S27) but is 710 the main driver of O<sub>3</sub> production above-canopy in pristine conditions (Fig. 7). The concentrated release of NO at sunrise facilitates greater O<sub>3</sub> production than if the same emissions were distributed across the day and is therefore important for capturing O<sub>3</sub> chemistry in pristine conditions.

715 NO<sub>x</sub> escape efficiencies are currently poorly constrained by observations. Comparison of single-layer parameterisations by Yienger and Levy (1995) to multilayer canopy calculations by (Ganzeveld et al., 2002b) find tropical forest escape efficiencies are highly sensitive to in-canopy NO<sub>x</sub> processes due to the role of chemistry and turbulence within the canopy. While single-layer estimates of 20% likely overestimate the role of deposition, the multilayer average from Ganzeveld et al. (2002b) of 40% is closer to our findings. We suggest that turbulence above the canopy is a good indicator of variability at this site without needing to resolve the full canopy structure and that resolution of the diurnal cycle in NO<sub>x</sub> escape is most important for representing the majority of the variability in escape efficiency.

#### 720 **3.4.2. The fate of upwind transported NO<sub>x</sub> within the canopy**

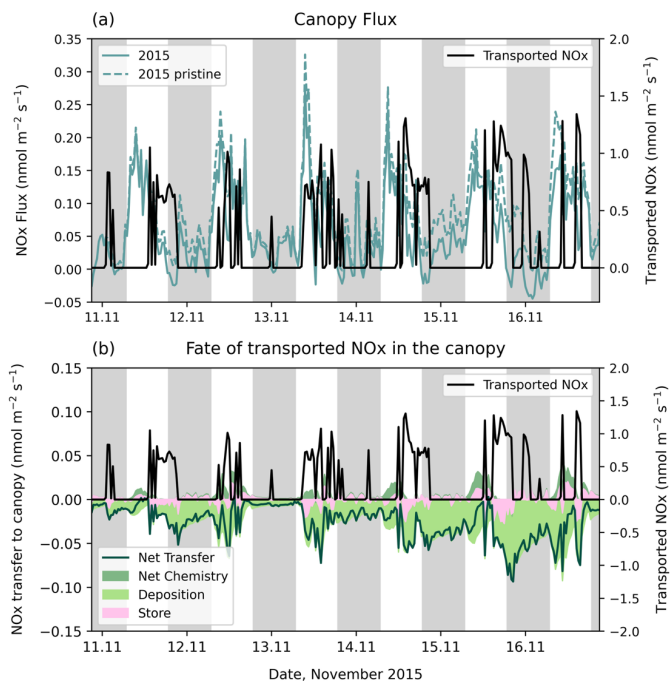
Here, we consider how transported NO<sub>2</sub> above the canopy in the 2015 period affects the total canopy NO<sub>x</sub> flux. When NO<sub>x</sub> concentrations above the canopy are high, as can happen when NO<sub>2</sub> is transported, the canopy can become a net sink. This bi-directional exchange means the canopy flux can switch from positive to negative in polluted conditions.

725 Figure 10a highlights the first 6 days of the simulation to show that even with transport of NO<sub>2</sub>, the canopy largely remains a NO<sub>x</sub> source. This is likely because NO<sub>x</sub> concentrations at the canopy top are not significantly enhanced in our simulations (Fig. S18). Exceptions occur when NO<sub>2</sub> transport occurs during the night; the transfer into the canopy at individual moments are greater than the soil NO escape, making the canopy a NO<sub>x</sub> sink (also see Fig. S27b). This implies the canopy must remain a substantial depositional sink overnight.

730 Figure 10b identifies the fate of transported NO<sub>x</sub> within the canopy to understand the source/sink behaviour. The instantaneous response to transported NO<sub>x</sub> within the canopy is an increase in canopy storage and deposition. After the NO<sub>2</sub> transport ends, there is often a reversal of storage (i.e., a release of NO<sub>x</sub>), although enhanced deposition continues. This is especially clear in

the daytime of the 16<sup>th</sup>. During the day, NO<sub>2</sub> transport often results in an almost instant transfer to the canopy, such that the net transfer follows the same pattern as spikes in upwind transport. This is due to efficient mixing into the canopy during the day. During the night, upwind NO<sub>2</sub> transport is not immediately transferred into the canopy, for example overnight transport events on the 13<sup>th</sup> and 14<sup>th</sup> do not show up as spikes in net canopy transfer. Instead, deposition is often spread throughout the night, especially if there has been significant transport of NO<sub>2</sub> to the site in the early evening (e.g., night of 15<sup>th</sup> and 16<sup>th</sup>). This is in response to NO<sub>2</sub> that was transferred into the canopy during the day and remains trapped due to nighttime stagnation of vertical mixing. In this way, the canopy response to NO<sub>2</sub> transport lasts longer than the actual transport event above the canopy and depends on the time of day. The daytime transfer is often too small relative to the soil flux to cause net loss of NO<sub>x</sub> to the canopy. During the night, however, sustained deposition of NO<sub>x</sub> trapped within the canopy transforms the top of canopy flux to a net sink.

Most single-layer canopy deposition schemes do not account for continued deposition of NO<sub>x</sub> stored within the canopy overnight. The resistance term includes an aerodynamic resistance that is lower when vertical turbulence is higher, describing enhanced transport into the canopy. However, a single-layer canopy cannot account for canopy storage, missing possible enhanced deposition of NO<sub>2</sub> during stagnant conditions overnight and may therefore underestimate NO<sub>x</sub> losses to the canopy.



750 **Figure 10:** (a) NO<sub>x</sub> transported from upwind above the canopy (black solid line) compared to the canopy-scale NO<sub>x</sub> flux in 2015 for simulations with transported NO<sub>2</sub> (teal solid line) and with pristine conditions (teal dashed line). (b) NO<sub>x</sub> transported from upwind above the canopy (black solid line) compared to transported NO<sub>x</sub> entering the canopy (green solid line), divided into deposition (light green shading), net chemistry (dark green shading) and storage (pink shading). Tick marks on the x axis are placed at midnight.

#### 4. Discussion

755 We demonstrate that a column model at the ATTO site in the remote Amazon successfully captures the greater meteorological and concentration gradients characteristic of deep tropical canopies, expanding previous applications in more well-mixed temperate forest (Ashworth et al., 2015; Wei et al., 2021). Notably, the model successfully simulates a 2-week period whereas previous studies were limited to two days.

760 The model reveals the critical role of transported precursors from biomass burning in the tropics. The flux of O<sub>3</sub> into the canopy is highest in 2015, attributed to O<sub>3</sub> production above the canopy from transported NO<sub>2</sub> from the Arc of Deforestation. The higher O<sub>3</sub> concentrations lead to greater sesquiterpene ozonolysis, reducing the sesquiterpene escape efficiency (Sect. 3.3)

whilst also decreasing the chemical loss velocity of O<sub>3</sub> (Fig. 5b). Because of the higher flux of freshly-formed O<sub>3</sub> into the canopy, absolute deposition and chemical losses increase (Fig. 5a). Biomass burning therefore increases stomatal O<sub>3</sub> flux, leading to a heightened risk of O<sub>3</sub> damage to the forest (e.g., Cheesman et al., 2024). We note that our representation of biomass burning by transport of upwind NO<sub>2</sub> is a substantial simplification; biomass burning is guaranteed to bring other trace gases not included in this simulation, which may impact background composition. Equally, wind arriving from the direction of the Arc of Deforestation has not necessarily passed through a biomass burning plume. Nonetheless, good representation of day-to-day variability in O<sub>3</sub> concentrations suggests this is a reasonable approximation (Fig. 3b).

Meteorological differences between simulation periods in 2013 and 2015 as a result of El Niño conditions, including higher temperatures and PAR in 2015, enhance BVOC emissions but produce only a small increase in canopy-scale O<sub>3</sub> deposition velocities (Fig. 5b). The sustained deposition velocities in the 2015 simulation suggest no significant stomatal limitation despite the extreme weather (Fig. 5b). Deposition schemes are highly parameterised and remain a substantial uncertainty in canopy modelling, and this study did not explore the leaf- or soil-level parameterisations in detail. As the majority of simulated O<sub>3</sub> and NO<sub>x</sub> canopy losses occur via this pathway, greater focus is needed on accurately representing deposition within the canopy and its response to changing meteorological conditions. Whilst stomata play a crucial role, non-stomatal deposition on plant surfaces also have an influence (Sun et al., 2016), but these are often represented, including here, by simple parameterisations in models. Previous studies have identified non-stomatal deposition to wet leaf surfaces to be a potentially relevant removal process in the tropics, an aspect not considered in this study (Yáñez-Serrano et al., 2018). The effect of canopy wetness on deposition magnitude and escape efficiencies may therefore be important for soluble BVOCs and NO<sub>x</sub>, and greater understanding of this process would enable improved parameterisations. Our simulations estimate sustained NO<sub>2</sub> deposition occurring overnight via non-stomatal pathways, leading to net canopy deposition when NO<sub>2</sub> is transported to the site (Fig. 10). Greater understanding of the partitioning between stomatal, cuticular and soil deposition is required to evaluate these conclusions.

Vertical turbulent mixing is a major contributor to variability in soil NO<sub>x</sub> escape efficiency (Fig. 9) and, to a lesser degree, in the escape efficiency of pool BVOCs and transfer of upwind NO<sub>2</sub> into the canopy; increased residence time within the canopy as a result of reduced mixing increases opportunities for chemical loss and deposition, decreasing escape efficiencies. Qualitatively, vertical mixing profiles are comparable to other measurements at Amazon sites (e.g., Freire et al., 2017; Santana et al., 2018) although representation of downdrafts and large-scale canopy sweeps (Bardakov et al., 2022; Unfer et al., 2025) are not possible with our parameterisation but can dominate the transport process at this site (Cava et al., 2022). We find intermittent turbulence is likely underestimated in our simulations at night. For a more explicit representation of vertical mixing processes, large eddy simulations (LES) that include a canopy should be explored (e.g., Pedruzo-Bagazgoitia et al., 2023).

Our simulations repeatedly highlight sesquiterpenes as dominant species in O<sub>3</sub> chemical removal within and above the canopy (Fig. 7). Nonetheless, further measurements of sesquiterpene species and reactivity are needed to accurately quantify the impact on O<sub>3</sub> concentrations. Sesquiterpene measurements are not currently available at the ATTO site, such that the emission factors used here could be better constrained if measurements become available. Similarly, monoterpene emissions can include

Formatted: Subscript

795 highly reactive species that have not been accurately characterised and our emission factors are estimated from observed  
concentration profiles rather than emission rate observations. We use the reactivity of  $\beta$ -caryophyllene to represent  
sesquiterpenes in our simulations, a species known for its high reactivity with  $O_3$ . This should be considered an upper limit on  
sesquiterpene contribution to reactivity, and therefore a lower limit on escape efficiency. Although  $\beta$ -caryophyllene is often a  
dominant species in measurements, farnesene, cadinenes, and muurolenes are frequently found to also be significant  
800 (Isaacman-VanWertz et al., 2024). A greater understanding of sesquiterpene emissions composition, and reactivity of other  
sesquiterpene classes would reduce uncertainty. Measuring the concentration of such highly reactive compounds in the  
atmosphere is severely hampered by their rapid decomposition; measurements must be taken close to the source. Our  
simulations also find that  $O_3$  reactivity with sesquiterpenes can continue above 100 m (Fig. 6), which suggests sesquiterpene  
concentration measurements may be possible above the canopy, especially in pristine conditions, which could help to constrain  
805 the model further.

In addition to the BVOCs investigated in this study, recent studies at ATTO show that oxygen-containing VOCs (OVOCs)  
contribute up to 22%–40% to the average OH reactivity, indicating the complexity of atmospheric oxidation (Ringsdorf et al.,  
2024), and that OVOCs have been underestimated as an important factor in the OH sink over the Amazon rainforest  
(Pfannerstill et al., 2021). Measurements at ATTO also show sesquiterpene emission from soils (Bourtsokidis et al., 2018) and  
810 cryptogams (Edtbauer et al., 2021): an initial estimate concluded they may contribute up to 10% of carbon emitted as VOCs  
in the form of highly reactive compounds (Kuhn et al., 2007). The processes from biological production to release to  
atmospheric fate, are highly complex, and more work is needed to investigate primary BVOC emissions at the leaf, branch  
and soil levels, track their atmospheric fate, and explore this complexity using models.

Similarly, the absence of reliable  $NO_x$  emissions and concentration measurements at the ATTO site prevents a direct evaluation  
815 of  $NO_x$  concentrations in the model. Missing  $\sigma_w$  data in 2013 likely also affected the model ability to faithfully simulate  
individual days. It is possible that by using  $\sigma_w$  from 2015 as a substitute, the average turbulence was too high, since some  
studies in the Amazon report 2015 as having increased turbulence compared to average years (Carneiro and Fisch, 2020;  
Pfannerstill et al., 2018). Additional measurements are required to refine the model and evaluate its accuracy under varying  
conditions across months, years, and seasons. We also identify a possible influence from biomass burning transport of  $NO_2$   
820 into the above-canopy space, so  $NO_x$  concentration measurements, especially during biomass burning months (the dry season),  
would help to refine this parameterisation. Further collaborative efforts between observation and modelling studies can help  
ensure data is collected in a way that is useful for multiple applications.

Finally, we consider the representation of these processes in global chemistry models. Whilst inclusion of multilayer canopies  
is becoming more common (e.g., Vermeuel et al., 2024), there remain many cases where single layer canopies are still (and  
825 will continue to be) in use due to computational constraints. [Already, simple canopy layer structures \(Makar et al., 2017\) and  
canopy layer parameterisations \(Wang et al., 2025\) are being implemented into large-scale models, highlighting a growing  
interest in representing in-canopy processes in computationally efficient ways.](#) Differences in in-canopy  $O_3$  chemistry between  
2013 and 2015 in our simulations only cause a small change in the canopy-scale deposition velocity, suggesting there is not

an urgent need for in-canopy chemical loss parameterisations that vary with environmental conditions. Similarly, explicit  
830 quantification of in-canopy sesquiterpene chemistry may not be essential for global modelling of O<sub>3</sub> as simulations without  
sesquiterpene emissions showed the O<sub>3</sub> + sesquiterpene reactions were compensated for via increased dry deposition (Fig. 5).  
These compensating effects of the canopy on above-canopy chemical composition in fact arise in multilayer canopies for  
several species and in response to various perturbations (Ganzeveld et al., 2010). Most global chemistry models exclude  
sesquiterpene chemistry due to uncertainties in their reactivity and the assumption that sesquiterpenes are removed within the  
835 canopy. Our model suggests that in pristine tropical environments approximately half of emissions can escape from the canopy  
and therefore may be relevant to boundary layer chemistry in global models, especially in pristine areas such as the tropics.  
Daily mean sesquiterpene escape efficiencies in our simulations qualitatively agree with existing escape efficiency  
parameterisations in global canopy-scale models (Guenther et al., 2006). Key factors affecting their escape are the degree of  
vertical mixing and the O<sub>3</sub> concentration (Fig. S25). For escape efficiencies of monoterpenes and isoprene, species with light-  
840 dependent emissions are the least sensitive to changes in in-canopy chemistry due to rapid mixing and equilibration during  
daylight – changes in oxidative capacity and depositional environment have a greater effect on the mean escape efficiency of  
species that build up overnight. Existing soil NO<sub>x</sub> parameterisations (Yienger and Levy, 1995) estimate greater in-canopy losses  
than our model; we calculate mean escape efficiencies of 40%–50%. We further agree with existing studies of pristine  
environments (e.g., Ganzeveld et al., 2002a, b) that a diurnally varying parameterisation of soil NO<sub>x</sub> escape could improve  
845 representation of variability in NO<sub>x</sub> chemistry; the diurnal cycle of soil NO<sub>x</sub> escape is strongly related to vertical turbulence,  
combined with an additional spike in morning escape efficiency that is important to consider for accurate simulation of O<sub>3</sub>  
production (Fig. 8).

## 5. Conclusion

Our column model application at the ATTO site successfully resolves key processes governing canopy–atmosphere exchange  
850 in the Amazon rainforest. The simulations capture interannual variability between simulation periods in 2013 and the 2015/16  
El Niño and reveal a previously underappreciated role of biomass burning in modulating canopy chemistry. Precursor transport  
from biomass burning enhances O<sub>3</sub> concentrations, reduces BVOC and NO<sub>x</sub> escape efficiencies, and alters O<sub>3</sub> chemical loss  
pathways. Sesquiterpenes, though exerting limited influence on total O<sub>3</sub> fluxes, play a key role in partitioning between chemical  
and depositional removal, introducing uncertainty due to poorly constrained emissions and reactivity. The uncertainty  
855 surrounding the role of sesquiterpenes is extremely high and research suggests that there are likely more sources than we  
include here. Variability in vertical mixing emerges as a dominant driver of both BVOC and NO<sub>x</sub> escape efficiencies, with  
implications for how these processes are represented in larger-scale models. Despite reasonable agreement with observations,  
uncertainties remain in emission magnitudes, chemical reactivity, and deposition parameterisations, emphasising the need for  
expanded in situ measurements, particularly of sesquiterpenes and soil NO<sub>x</sub> fluxes. Future work coupling column or LES  
860 frameworks that include vegetation with long-term, multi-seasonal datasets will be essential to refine canopy exchange  
parameterisations and to improve predictions of tropical forest responses to climatic and atmospheric perturbations. Given the

potential for shifts in fire activity, dry season length, and BVOC emissions under future climate scenarios, improved treatment of in-canopy processes will be essential for constraining tropical atmospheric chemistry and its role in regional and global oxidant budgets.

865

**Data availability:** Data and scripts to reproduce all figures will be stored with DOI on a Zenodo archive following review.

The column model with adaptations for the ATTO site is available on github ([https://github.com/flossie-brown/FORCAST\\_ATTO](https://github.com/flossie-brown/FORCAST_ATTO)). [Max Planck Institute for Chemistry acknowledges financial support from the Max Planck Society and the Bundesministerium für Bildung und Forschung.](#)

870

Observation data is available at [www.attodata.org](http://www.attodata.org).

**Author contribution:**

Conceptualisation: FB, CLH

Supervision: CLH

Analysis & Visualisation: FB

875

Writing – first draft: FB

Writing: FB, CLH

Resources: AS, HH, CAM, AMYS, JK, ACA, CQDJ, DHH, [SW](#)

Writing – review & editing: all authors

**Competing interests:** The authors declare that they have no conflict of interest.

880

**Acknowledgements:** ATTO scientists thank the Instituto Nacional de Pesquisas da Amazonia (INPA) and the Max Planck Society for continuous support. We acknowledge the support by the German Federal Ministry of Education and Research (BMBF contracts 01LB1001A and 01LK1602B) and the Brazilian Ministério da Ciência, Tecnologia e Inovação (MCTI/FINEP contract 01.11.01248.00) as well as the Amazon State University (UEA), FAPEAM, LBA/INPA and SDS/CEUC/RDS-Uatumã.)

885

**References:**

Andreae, M. O., Acevedo, O. C., Araújo, A., Artaxo, P., Barbosa, C. G. G., Barbosa, H. M. J., Brito, J., Carbone, S., Chi, X., Cintra, B. B. L., da Silva, N. F., Dias, N. L., Dias-Júnior, C. Q., Ditas, F., Ditz, R., Godoi, A. F. L., Godoi, R. H. M., Heimann, M., Hoffmann, T., Kesselmeier, J., Könemann, T., Krüger, M. L., Lavric, J. V., Manzi, A. O., Lopes, A. P., Martins, D. L., Mikhailov, E. F., Moran-Zuloaga, D., Nelson, B. W., Nölscher, A. C., Santos Nogueira, D., Piedade, M. T. F., Pöhlker, C., Pöschl, U., Quesada, C. A., Rizzo, L. V., Ro, C.-U., Ruckteschler, N., Sá, L. D. A., de Oliveira Sá, M., Sales, C. B., dos Santos, R. M. N., Saturno, J., Schöngart, J., Sörgel, M., de Souza, C. M., de Souza, R. a. F., Su, H., Targhetta, N., Tóta, J., Trebs, I., Trumbore, S., van Eijck, A., Walter, D., Wang, Z., Weber, B., Williams, J., Winderlich, J., Wittmann, F., Wolff, S., and Yáñez-Serrano, A. M.: The Amazon Tall Tower Observatory (ATTO): overview of pilot measurements on ecosystem ecology, meteorology, trace gases, and aerosols, *Atmospheric Chemistry and Physics*, 15, 10723–10776, <https://doi.org/10.5194/acp-15-10723-2015>, 2015.

895

Formatted: Font: Times New Roman, 10 pt, Font color: Text 1, English (US)

- Aragão, L. E., Anderson, L. O., Fonseca, M. G., Rosan, T. M., Vedovato, L. B., Wagner, F. H., Silva, C. V., Silva Junior, C. H., Arai, E., and Aguiar, A. P.: 21st Century drought-related fires counteract the decline of Amazon deforestation carbon emissions, *Nature communications*, 9, 536, 2018.
- Ashworth, K., Chung, S. H., Griffin, R. J., Chen, J., Forkel, R., Bryan, A. M., and Steiner, A. L.: FORest Canopy Atmosphere Transfer (FORCAST) 1.0: a 1-D model of biosphere-atmosphere chemical exchange, *Geosci. Model Dev.*, 8, 3765–3784, <https://doi.org/10.5194/gmd-8-3765-2015>, 2015.
- Bakwin, P. S., Wofsy, S. C., Fan, S.-M., Keller, M., Trumbore, S. E., and Da Costa, J. M.: Emission of nitric oxide (NO) from tropical forest soils and exchange of NO between the forest canopy and atmospheric boundary layers, *Journal of Geophysical Research: Atmospheres*, 95, 16755–16764, <https://doi.org/10.1029/JD095iD10p16755>, 1990.
- Bardakov, R., Krejci, R., Riipinen, I., and Ekman, A. M. L.: The Role of Convective Up- and Downdrafts in the Transport of Trace Gases in the Amazon, *Journal of Geophysical Research: Atmospheres*, 127, e2022JD037265, <https://doi.org/10.1029/2022JD037265>, 2022.
- [Botía, S., Gerbig, C., Marshall, J., Lavric, J. V., Walter, D., Pöhlker, C., Holanda, B., Fisch, G., de Araújo, A. C., Sá, M. O., Teixeira, P. R., Resende, A. F., Dias-Junior, C. Q., van Asperen, H., Oliveira, P. S., Stefanello, M., and Acevedo, O. C.: Understanding nighttime methane signals at the Amazon Tall Tower Observatory \(ATTO\), \*Atmospheric Chemistry and Physics\*, 20, 6583–6606, <https://doi.org/10.5194/acp-20-6583-2020>, 2020.](#)
- [Botía, S., Komiya, S., Marshall, J., Koch, T., Gałkowski, M., Lavric, J., Gomes-Alves, E., Walter, D., Fisch, G., Pinho, D. M., Nelson, B. W., Martins, G., Luijkx, I. T., Koren, G., Florentie, L., Carioca de Araújo, A., Sá, M., Andreae, M. O., Heimann, M., Peters, W., and Gerbig, C.: The CO<sub>2</sub> record at the Amazon Tall Tower Observatory: A new opportunity to study processes on seasonal and inter-annual scales, \*Global Change Biology\*, 28, 588–611, <https://doi.org/10.1111/gcb.15905>, 2022.](#)
- Bourtsoukidis, E., Behrendt, T., Yañez-Serrano, A. M., Hellén, H., Diamantopoulos, E., Catão, E., Ashworth, K., Pozzer, A., Quesada, C. A., Martins, D. L., Sá, M., Araujo, A., Brito, J., Artaxo, P., Kesselmeier, J., Lelieveld, J., and Williams, J.: Strong sesquiterpene emissions from Amazonian soils, *Nat Commun*, 9, 2226, <https://doi.org/10.1038/s41467-018-04658-y>, 2018.
- Breuninger, C., Meixner, F. X., and Kesselmeier, J.: Field investigations of nitrogen dioxide (NO<sub>2</sub>) exchange between plants and the atmosphere, *Atmospheric Chemistry and Physics*, 13, 773–790, <https://doi.org/10.5194/acp-13-773-2013>, 2013.
- Brown, F., Folberth, G. A., Sitch, S., Bauer, S., Bauters, M., Boeckx, P., Cheesman, A. W., Deushi, M., Dos Santos Vieira, I., Galy-Lacaux, C., Haywood, J., Keeble, J., Mercado, L. M., O'Connor, F. M., Oshima, N., Tsigaridis, K., and Verbeeck, H.: The ozone-climate penalty over South America and Africa by 2100, *Atmospheric Chemistry and Physics*, 22, 12331–12352, <https://doi.org/10.5194/acp-22-12331-2022>, 2022.
- Bryan, A. M., Bertman, S. B., Carroll, M. A., Dusanter, S., Edwards, G. D., Forkel, R., Griffith, S., Guenther, A. B., Hansen, R. F., Helmig, D., Jobson, B. T., Keutsch, F. N., Lefer, B. L., Pressley, S. N., Shepson, P. B., Stevens, P. S., and Steiner, A. L.: In-canopy gas-phase chemistry during CABINEX 2009: sensitivity of a 1-D canopy model to vertical mixing and isoprene chemistry, *Atmospheric Chemistry and Physics*, 12, 8829–8849, <https://doi.org/10.5194/acp-12-8829-2012>, 2012.
- Cárdenas, L., Rondón, A., Johansson, C., and Sanhueza, E.: Effects of soil moisture, temperature, and inorganic nitrogen on nitric oxide emissions from acidic tropical savannah soils, *Journal of Geophysical Research: Atmospheres*, 98, 14783–14790, <https://doi.org/10.1029/93JD01020>, 1993.
- Carneiro, R. G. and Fisch, G.: Observational analysis of the daily cycle of the planetary boundary layer in the central Amazon during a non-El Niño year and El Niño year (GoAmazon project 2014/5), *Atmospheric Chemistry and Physics*, 20, 5547–5558, <https://doi.org/10.5194/acp-20-5547-2020>, 2020.

- 935 Cava, D., Dias-Júnior, C. Q., Acevedo, O., Oliveira, P. E. S., Tsokankunku, A., Sörgel, M., Manzi, A. O., de Araújo, A. C., Brondani, D. V., Toro, I. M. C., and Mortarini, L.: Vertical propagation of submeso and coherent structure in a tall and dense Amazon Forest in different stability conditions PART I: Flow structure within and above the roughness sublayer, *Agricultural and Forest Meteorology*, 322, 108983, <https://doi.org/10.1016/j.agrformet.2022.108983>, 2022.
- 940 Chamecki, M., Freire, L. S., Dias, N. L., Chen, B., Dias-Junior, C. Q., Machado, L. A. T., Sörgel, M., Tsokankunku, A., and Araújo, A. C. de: Effects of Vegetation and Topography on the Boundary Layer Structure above the Amazon Forest, *Journal of the Atmospheric Sciences*, 77, 2941–2957, <https://doi.org/10.1175/JAS-D-20-0063.1>, 2020.
- Chaparro-Suarez, I. G., Meixner, F. X., and Kesselmeier, J.: Nitrogen dioxide (NO<sub>2</sub>) uptake by vegetation controlled by atmospheric concentrations and plant stomatal aperture, *Atmospheric Environment*, 45, 5742–5750, <https://doi.org/10.1016/j.atmosenv.2011.07.021>, 2011.
- 945 Cheesman, A. W., Brown, F., Artaxo, P., Farha, M. N., Folberth, G. A., Hayes, F. J., Heinrich, V. H., Hill, T. C., Mercado, L. M., and Oliver, R. J.: Reduced productivity and carbon drawdown of tropical forests from ground-level ozone exposure, *Nature Geoscience*, 17, 1003–1007, 2024.
- Clifton, O. E., Schwede, D., Hogrefe, C., Bash, J. O., Bland, S., Cheung, P., Coyle, M., Emberson, L., Flemming, J., Fredj, E., Galmarini, S., Ganzeveld, L., Gazetas, O., Goded, I., Holmes, C. D., Horváth, L., Huijnen, V., Li, Q., Makar, P. A., Mammarella, I., Manca, G., Munger, J. W., Pérez-Camanyo, J. L., Pleim, J., Ran, L., San Jose, R., Silva, S. J., Staebler, R., Sun, S., Tai, A. P. K., Tas, E., Vesala, T., Weidinger, T., Wu, Z., and Zhang, L.: A single-point modeling approach for the intercomparison and evaluation of ozone dry deposition across chemical transport models (Activity 2 of AQMEII4), *Atmospheric Chemistry and Physics*, 23, 9911–9961, <https://doi.org/10.5194/acp-23-9911-2023>, 2023.
- 950 Cordova, A. M., Longo, K., Freitas, S., Gatti, L. V., Artaxo, P., Procópio, A., Silva Dias, M. a. F., and Freitas, E. D.: Nitrogen oxides measurements in an Amazon site and enhancements associated with a cold front, *Atmospheric Chemistry and Physics Discussions*, 4, 2301–2331, <https://doi.org/10.5194/acpd-4-2301-2004>, 2004.
- Costa, B., Anselmo-Moreira, F., Nascimento, A., Pedrosa, G., Catharino, E., Borbon, A., Fornaro, A., Furlan, C., and Souza, S. de: Unveiling Sesquiterpene Emissions in Dominant Trees of a Brazilian Atlantic Forest Remnant, <https://doi.org/10.26434/chemrxiv-2025-8pg46>, 17 April 2025.
- 960 Covey, K., Soper, F., Pangala, S., Bernardino, A., Pagliaro, Z., Basso, L., Cassol, H., Fearnside, P., Navarrete, D., Novoa, S., Sawakuchi, H., Lovejoy, T., Marengo, J., Peres, C. A., Baillie, J., Bernasconi, P., Camargo, J., Freitas, C., Hoffman, B., Nardoto, G. B., Nobre, I., Mayorga, J., Mesquita, R., Pavan, S., Pinto, F., Rocha, F., de Assis Mello, R., Thuault, A., Bahl, A. A., and Elmore, A.: Carbon and Beyond: The Biogeochemistry of Climate in a Rapidly Changing Amazon, *Front. For. Glob. Change*, 4, <https://doi.org/10.3389/ffgc.2021.618401>, 2021.
- 965 Dias-Júnior, C. Q., Dias, N. L., dos Santos, R. M. N., Sörgel, M., Araújo, A., Tsokankunku, A., Ditas, F., de Santana, R. A., von Randow, C., Sá, M., Pöhlker, C., Toledo Machado, L. A., de Sá, L. D., Moran-Zuloaga, D., Janssen, R., Acevedo, O., Oliveira, P., Fisch, G., Chor, T., and Manzi, A.: Is There a Classical Inertial Sublayer Over the Amazon Forest?, *Geophysical Research Letters*, 46, 5614–5622, <https://doi.org/10.1029/2019GL083237>, 2019.
- 970 Edtbauer, A., Pfannerstill, E. Y., Pires Florentino, A. P., Barbosa, C. G. G., Rodriguez-Caballero, E., Zannoni, N., Alves, R. P., Wolff, S., Tsokankunku, A., Aptroot, A., de Oliveira Sá, M., de Araújo, A. C., Sörgel, M., de Oliveira, S. M., Weber, B., and Williams, J.: Cryptogamic organisms are a substantial source and sink for volatile organic compounds in the Amazon region, *Commun Earth Environ*, 2, 258, <https://doi.org/10.1038/s43247-021-00328-y>, 2021.
- Erickson, H., Davidson, E. A., and Keller, M.: Former land-use and tree species affect nitrogen oxide emissions from a tropical dry forest, *Oecologia*, 130, 297–308, <https://doi.org/10.1007/s004420100801>, 2002.

- 975 Forkel, R., Klemm, O., Graus, M., Rappenglück, B., Stockwell, W. R., Grabmer, W., Held, A., Hansel, A., and Steinbrecher, R.: Trace gas exchange and gas phase chemistry in a Norway spruce forest: A study with a coupled 1-dimensional canopy atmospheric chemistry emission model, *Atmospheric Environment*, 40, 28–42, <https://doi.org/10.1016/j.atmosenv.2005.11.070>, 2006.
- Freire, L. S., Gerken, T., Ruiz-Plancarte, J., Wei, D., Fuentes, J. D., Katul, G. G., Dias, N. L., Acevedo, O. C., and Chamecki, M.: Turbulent mixing and removal of ozone within an Amazon rainforest canopy, *Journal of Geophysical Research: Atmospheres*, 122, 2791–2811, <https://doi.org/10.1002/2016JD026009>, 2017.
- 980 Ganzeveld, L., Bouwman, L., Stehfest, E., van Vuuren, D. P., Eickhout, B., and Lelieveld, J.: Impact of future land use and land cover changes on atmospheric chemistry-climate interactions, *Journal of Geophysical Research: Atmospheres*, 115, <https://doi.org/10.1029/2010JD014041>, 2010.
- 985 Ganzeveld, L. N., Lelieveld, J., Dentener, F. J., Krol, M. C., and Roelofs, G.-J.: Atmosphere-biosphere trace gas exchanges simulated with a single-column model, *Journal of Geophysical Research: Atmospheres*, 107, ACH 8-1-ACH 8-21, <https://doi.org/10.1029/2001JD000684>, 2002a.
- Ganzeveld, L. N., Lelieveld, J., Dentener, F. J., Krol, M. C., Bouwman, A. J., and Roelofs, G.-J.: Global soil-biogenic NO<sub>x</sub> emissions and the role of canopy processes, *Journal of Geophysical Research: Atmospheres*, 107, ACH 9-1-ACH 9-17, <https://doi.org/10.1029/2001JD001289>, 2002b.
- 990 Gao, W., Wesely, M. L., and Doskey, P. V.: Numerical modeling of the turbulent diffusion and chemistry of NO<sub>x</sub>, O<sub>3</sub>, isoprene, and other reactive trace gases in and above a forest canopy, *Journal of Geophysical Research: Atmospheres*, 98, 18339–18353, <https://doi.org/10.1029/93JD01862>, 1993.
- Gerken, T., Ruddell, B. L., Fuentes, J. D., Araújo, A., Brunzell, N. A., Maia, J., Manzi, A., Mercer, J., dos Santos, R. N., von Randow, C., and Stoy, P. C.: Investigating the mechanisms responsible for the lack of surface energy balance closure in a central Amazonian tropical rainforest, *Agricultural and Forest Meteorology*, 255, 92–103, <https://doi.org/10.1016/j.agrformet.2017.03.023>, 2018.
- 995 Gomes Alves, E., Taylor, T., Robin, M., Pinheiro Oliveira, D., Schiatti, J., Duvoisin Júnior, S., Zannoni, N., Williams, J., Hartmann, C., Gonçalves, J. F. C., Schöngart, J., Wittmann, F., and Piedade, M. T. F.: Seasonal shifts in isoprenoid emission composition from three hyperdominant tree species in central Amazonia, *Plant Biology*, 24, 721–733, <https://doi.org/10.1111/plb.13419>, 2022.
- 1000 Gomes Alves, E., Aquino Santana, R., Quaresma Dias-Júnior, C., Botía, S., Taylor, T., Yáñez-Serrano, A. M., Kesselmeier, J., Bourtsoukidis, E., Williams, J., Lembo Silveira de Assis, P. I., Martins, G., de Souza, R., Duvoisin Júnior, S., Guenther, A., Gu, D., Tsokankunku, A., Sörgel, M., Nelson, B., Pinto, D., Komiya, S., Martins Rosa, D., Weber, B., Barbosa, C., Robin, M., Feeley, K. J., Duque, A., Londoño Lemos, V., Contreras, M. P., Idarraga, A., López, N., Husby, C., Jestrow, B., and Cely Toro, I. M.: Intra- and interannual changes in isoprene emission from central Amazonia, *Atmospheric Chemistry and Physics*, 23, 8149–8168, <https://doi.org/10.5194/acp-23-8149-2023>, 2023.
- 1005 Guenther, A., Hewitt, C. N., Erickson, D., Fall, R., Geron, C., Graedel, T., Harley, P., Klinger, L., Lerdau, M., Mckay, W. A., Pierce, T., Scholes, B., Steinbrecher, R., Tallamraju, R., Taylor, J., and Zimmerman, P.: A global model of natural volatile organic compound emissions, *Journal of Geophysical Research: Atmospheres*, 100, 8873–8892, <https://doi.org/10.1029/94JD02950>, 1995.
- 1010 Guenther, A., Karl, T., Harley, P., Wiedinmyer, C., Palmer, P. I., and Geron, C.: Estimates of global terrestrial isoprene emissions using MEGAN (Model of Emissions of Gases and Aerosols from Nature), *Atmospheric Chemistry and Physics*, 6, 3181–3210, <https://doi.org/10.5194/acp-6-3181-2006>, 2006.

- 1015 Guenther, A. B., Jiang, X., Heald, C. L., Sakulyanontvittaya, T., Duhl, T., Emmons, L. K., and Wang, X.: The Model of Emissions of Gases and Aerosols from Nature version 2.1 (MEGAN2.1): an extended and updated framework for modeling biogenic emissions, *Geoscientific Model Development*, 5, 1471–1492, <https://doi.org/10.5194/gmd-5-1471-2012>, 2012.
- Gut, A., Scheibe, M., Rottenberger, S., Rummel, U., Welling, M., Ammann, C., Kirkman, G. A., Kuhn, U., Meixner, F. X., Kesselmeier, J., Lehmann, B. E., Schmidt, W., Müller, E., and Piedade, M. T. F.: Exchange fluxes of NO<sub>2</sub> and O<sub>3</sub> at soil and leaf surfaces in an Amazonian rain forest, *Journal of Geophysical Research: Atmospheres*, 107, LBA 27-1-LBA 27-15, <https://doi.org/10.1029/2001JD000654>, 2002.
- 1020
- Hudman, R. C., Moore, N. E., Mebust, A. K., Martin, R. V., Russell, A. R., Valin, L. C., and Cohen, R. C.: Steps towards a mechanistic model of global soil nitric oxide emissions: implementation and space based-constraints, *Atmospheric Chemistry and Physics*, 12, 7779–7795, <https://doi.org/10.5194/acp-12-7779-2012>, 2012.
- 1025
- Isaacman-VanWertz, G., Frazier, G., Willison, J., and Faiola, C.: Missing Measurements of Sesquiterpene Ozonolysis Rates and Composition Limit Understanding of Atmospheric Reactivity, *Environ. Sci. Technol.*, <https://doi.org/10.1021/acs.est.3c10348>, 2024.
- Jardine, K., Yañez Serrano, A., Arneth, A., Abrell, L., Jardine, A., van Haren, J., Artaxo, P., Rizzo, L. V., Ishida, F. Y., Karl, T., Kesselmeier, J., Saleska, S., and Huxman, T.: Within-canopy sesquiterpene ozonolysis in Amazonia, *Journal of Geophysical Research: Atmospheres*, 116, <https://doi.org/10.1029/2011JD016243>, 2011.
- 1030
- Jarvis, P. G.: The interpretation of the variations in leaf water potential and stomatal conductance found in canopies in the field, *Philos Trans R Soc Lond B Biol Sci*, 273, 593–610, <https://doi.org/10.1098/rstb.1976.0035>, 1976.
- Jiménez-Muñoz, J. C., Mattar, C., Barichivich, J., Santamaría-Artigas, A., Takahashi, K., Malhi, Y., Sobrino, J. A., and Schrier, G. van der: Record-breaking warming and extreme drought in the Amazon rainforest during the course of El Niño 2015–2016, *Sci Rep*, 6, 33130, <https://doi.org/10.1038/srep33130>, 2016.
- 1035
- Ke, P., Kang, R., Avery, L. K., Zhang, J., Yu, Q., Xie, D., and Duan, L.: Temporal variations of soil NO and NO<sub>2</sub> fluxes in two typical subtropical forests receiving contrasting rates of N deposition, *Environmental Pollution*, 295, 118696, <https://doi.org/10.1016/j.envpol.2021.118696>, 2022.
- Kuhn, U., Rottenberger, S., Biesenthal, T., Wolf, A., Schebeske, G., Ciccioli, P., Brancaleoni, E., Frattoni, M., Tavares, T. M., and Kesselmeier, J.: Seasonal differences in isoprene and light-dependent monoterpene emission by Amazonian tree species, *Global Change Biology*, 10, 663–682, <https://doi.org/10.1111/j.1529-8817.2003.00771.x>, 2004a.
- 1040
- Kuhn, U., Rottenberger, S., Biesenthal, T., Wolf, A., Schebeske, G., Ciccioli, P., and Kesselmeier, J.: Strong correlation between isoprene emission and gross photosynthetic capacity during leaf phenology of the tropical tree species *Hymenaea courbaril* with fundamental changes in volatile organic compounds emission composition during early leaf development, *Plant, Cell & Environment*, 27, 1469–1485, <https://doi.org/10.1111/j.1365-3040.2004.01252.x>, 2004b.
- 1045
- Kuhn, U., Andreae, M. O., Ammann, C., Araújo, A. C., Brancaleoni, E., Ciccioli, P., Dindorf, T., Frattoni, M., Gatti, L. V., Ganzeveld, L., Kruijt, B., Lelieveld, J., Lloyd, J., Meixner, F. X., Nobre, A. D., Pöschl, U., Spirig, C., Stefani, P., Thielmann, A., Valentini, R., and Kesselmeier, J.: Isoprene and monoterpene fluxes from Central Amazonian rainforest inferred from tower-based and airborne measurements, and implications on the atmospheric chemistry and the local carbon budget, *Atmospheric Chemistry and Physics*, 7, 2855–2879, <https://doi.org/10.5194/acp-7-2855-2007>, 2007.
- 1050
- Lee, B. H., Munger, J. W., Wofsy, S. C., Rizzo, L. V., Yoon, J. Y. S., Turner, A. J., Thornton, J. A., and Swann, A. L. S.: Sensitive Response of Atmospheric Oxidative Capacity to the Uncertainty in the Emissions of Nitric Oxide (NO) From Soils in Amazonia, *Geophysical Research Letters*, 51, e2023GL107214, <https://doi.org/10.1029/2023GL107214>, 2024.

- 1055 Luo, G. J., Kiese, R., Wolf, B., and Butterbach-Bahl, K.: Effects of soil temperature and moisture on methane uptake and nitrous oxide emissions across three different ecosystem types, *Biogeosciences*, 10, 3205–3219, <https://doi.org/10.5194/bg-10-3205-2013>, 2013.
- Makar, P. A., Fuentes, J. D., Wang, D., Staebler, R. M., and Wiebe, H. A.: Chemical processing of biogenic hydrocarbons within and above a temperate deciduous forest, *Journal of Geophysical Research: Atmospheres*, 104, 3581–3603, <https://doi.org/10.1029/1998JD100065>, 1999.
- 1060 Makar, P. A., Staebler, R. M., Akingunola, A., Zhang, J., McLinden, C., Kharol, S. K., Pabla, B., Cheung, P., and Zheng, Q.: The effects of forest canopy shading and turbulence on boundary layer ozone, *Nat Commun*, 8, 15243, <https://doi.org/10.1038/ncomms15243>, 2017.
- Marengo, J. A., Souza, C. M., Thonicke, K., Burton, C., Halladay, K., Betts, R. A., Alves, L. M., and Soares, W. R.: Changes in Climate and Land Use Over the Amazon Region: Current and Future Variability and Trends, *Front. Earth Sci.*, 6, 1065 <https://doi.org/10.3389/feart.2018.00228>, 2018.
- Mortarini, L., Dias-Júnior, C. Q., Acevedo, O., Oliveira, P. E. S., Tsokankunku, A., Sörgel, M., Manzi, A. O., de Araújo, A. C., Brondani, D. V., Toro, I. M. C., Giostra, U., and Cava, D.: Vertical propagation of submeso and coherent structure in a tall and dense amazon forest in different stability conditions. PART II: Coherent structures analysis, *Agricultural and Forest Meteorology*, 322, 108993, <https://doi.org/10.1016/j.agrformet.2022.108993>, 2022.
- 1070 Otu-Larbi, F., Conte, A., Fares, S., Wild, O., and Ashworth, K.: FORCAsT-gs: Importance of Stomatal Conductance Parameterization to Estimated Ozone Deposition Velocity, *Journal of Advances in Modeling Earth Systems*, 13, e2021MS002581, <https://doi.org/10.1029/2021MS002581>, 2021.
- Pacifico, F., Folberth, G., Sitch, S., Haywood, J., Rizzo, L., Malavelle, F., and Artaxo, P.: Biomass burning related ozone damage on vegetation over the Amazon forest: a model sensitivity study, *Atmospheric Chemistry and Physics*, 15, 2791–2804, 1075 2015.
- Pedruzo-Bagazgoitia, X., Patton, E. G., Moene, A. F., Ouwersloot, H. G., Gerken, T., Machado, L. a. T., Martin, S. T., Sörgel, M., Stoy, P. C., Yamasoe, M. A., and Vilà-Guerau de Arellano, J.: Investigating the Diurnal Radiative, Turbulent, and Biophysical Processes in the Amazonian Canopy-Atmosphere Interface by Combining LES Simulations and Observations, *Journal of Advances in Modeling Earth Systems*, 15, e2022MS003210, <https://doi.org/10.1029/2022MS003210>, 2023.
- 1080 Pfannerstill, E. Y., Nölscher, A. C., Yáñez-Serrano, A. M., Boursoukakis, E., Keßel, S., Janssen, R. H. H., Tsokankunku, A., Wolff, S., Sörgel, M., Sá, M. O., Araújo, A., Walter, D., Lavrič, J., Dias-Júnior, C. Q., Kesselmeier, J., and Williams, J.: Total OH Reactivity Changes Over the Amazon Rainforest During an El Niño Event, *Front. For. Glob. Change*, 1, <https://doi.org/10.3389/ffgc.2018.00012>, 2018.
- 1085 Pfannerstill, E. Y., Reijrink, N. G., Edtbauer, A., Ringsdorf, A., Zannoni, N., Araújo, A., Ditas, F., Holanda, B. A., Sá, M. O., Tsokankunku, A., Walter, D., Wolff, S., Lavrič, J. V., Pöhlker, C., Sörgel, M., and Williams, J.: Total OH reactivity over the Amazon rainforest: variability with temperature, wind, rain, altitude, time of day, season, and an overall budget closure, *Atmospheric Chemistry and Physics*, 21, 6231–6256, <https://doi.org/10.5194/acp-21-6231-2021>, 2021.
- 1090 Pöhlker, C., Walter, D., Paulsen, H., Könemann, T., Rodríguez-Caballero, E., Moran-Zuloaga, D., Brito, J., Carbone, S., Degrendele, C., Després, V. R., Ditas, F., Holanda, B. A., Kaiser, J. W., Lammel, G., Lavrič, J. V., Ming, J., Pickersgill, D., Pöhlker, M. L., Praß, M., Löbs, N., Saturno, J., Sörgel, M., Wang, Q., Weber, B., Wolff, S., Artaxo, P., Pöschl, U., and Andreae, M. O.: Land cover and its transformation in the backward trajectory footprint region of the Amazon Tall Tower Observatory, *Atmospheric Chemistry and Physics*, 19, 8425–8470, <https://doi.org/10.5194/acp-19-8425-2019>, 2019.

- Pöhlker, M. L., Ditas, F., Saturno, J., Klimach, T., Hrabě de Angelis, I., Araújo, A. C., Brito, J., Carbone, S., Cheng, Y., Chi, X., Ditz, R., Gunthe, S. S., Holanda, B. A., Kandler, K., Kesselmeier, J., Könemann, T., Krüger, O. O., Lavrič, J. V., Martin, S. T., Mikhailov, E., Moran-Zuloaga, D., Rizzo, L. V., Rose, D., Su, H., Thalman, R., Walter, D., Wang, J., Wolff, S., Barbosa, H. M. J., Artaxo, P., Andreae, M. O., Pöschl, U., and Pöhlker, C.: Long-term observations of cloud condensation nuclei over the Amazon rain forest – Part 2: Variability and characteristics of biomass burning, long-range transport, and pristine rain forest aerosols, *Atmospheric Chemistry and Physics*, 18, 10289–10331, <https://doi.org/10.5194/acp-18-10289-2018>, 2018.
- 1095 Pope, R. J., Arnold, S. R., Chipperfield, M. P., Reddington, C. L. S., Butt, E. W., Keslake, T. D., Feng, W., Latter, B. G., Kerridge, B. J., Siddans, R., Rizzo, L., Artaxo, P., Sadiq, M., and Tai, A. P. K.: Substantial Increases in Eastern Amazon and Cerrado Biomass Burning-Sourced Tropospheric Ozone, *Geophysical Research Letters*, 47, e2019GL084143, <https://doi.org/10.1029/2019GL084143>, 2020.
- Pugliese, G., Ingrisch, J., Meredith, L. K., Pfannerstill, E. Y., Klüpfel, T., Meeran, K., Byron, J., Purser, G., Gil-Loaiza, J., van Haren, J., Dontsova, K., Kreuzwieser, J., Ladd, S. N., Werner, C., and Williams, J.: Effects of drought and recovery on soil volatile organic compound fluxes in an experimental rainforest, *Nat Commun*, 14, 5064, <https://doi.org/10.1038/s41467-023-40661-8>, 2023.
- 1105 Raupach, M. R.: A practical Lagrangian method for relating scalar concentrations to source distributions in vegetation canopies, *Quarterly Journal of the Royal Meteorological Society*, 115, 609–632, <https://doi.org/10.1002/qj.49711548710>, 1989.
- dos Reis, M., Graça, P. M. L. de A., Yanai, A. M., Ramos, C. J. P., and Fearnside, P. M.: Forest fires and deforestation in the central Amazon: Effects of landscape and climate on spatial and temporal dynamics, *Journal of Environmental Management*, 288, 112310, <https://doi.org/10.1016/j.jenvman.2021.112310>, 2021.
- Restrepo-Coupe, N., Albert, L. P., Longo, M., Baker, I., Levine, N. M., Mercado, L. M., da Araujo, A. C., Christoffersen, B. O., Costa, M. H., Fitzjarrald, D. R., Galbraith, D., Imbuzeiro, H., Malhi, Y., von Randow, C., Zeng, X., Moorcroft, P., and Saleska, S. R.: Understanding water and energy fluxes in the Amazonia: Lessons from an observation-model intercomparison, *Global Change Biology*, 27, 1802–1819, <https://doi.org/10.1111/gcb.15555>, 2021.
- 1115 Ribeiro Neto, G. G., Anderson, L. O., Barretos, N. J. C., Abreu, R., Alves, L., Dong, B., Lott, F. C., and Tett, S. F. B.: Attributing the 2015/2016 Amazon basin drought to anthropogenic influence, *Climate Resilience and Sustainability*, 1, e25, <https://doi.org/10.1002/cli2.25>, 2022.
- Ringsdorf, A., Edtbauer, A., Holanda, B., Pöhlker, C., Sá, M. O., Araújo, A., Kesselmeier, J., Lelieveld, J., and Williams, J.: Investigating carbonyl compounds above the Amazon rainforest using a proton-transfer-reaction time-of-flight mass spectrometer (PTR-ToF-MS) with NO<sup>+</sup> chemical ionization, *Atmospheric Chemistry and Physics*, 24, 11883–11910, <https://doi.org/10.5194/acp-24-11883-2024>, 2024.
- Rummel, U., Ammann, C., Gut, A., Meixner, F. X., and Andreae, M. O.: Eddy covariance measurements of nitric oxide flux within an Amazonian rain forest, *Journal of Geophysical Research: Atmospheres*, 107, LBA 17-1-LBA 17-9, <https://doi.org/10.1029/2001JD000520>, 2002.
- 1125 Rummel, U., Ammann, C., Kirkman, G. A., Moura, M. a. L., Foken, T., Andreae, M. O., and Meixner, F. X.: Seasonal variation of ozone deposition to a tropical rain forest in southwest Amazonia, *Atmospheric Chemistry and Physics*, 7, 5415–5435, <https://doi.org/10.5194/acp-7-5415-2007>, 2007.
- Santana, R. A., Dias-Júnior, C. Q., da Silva, J. T., Fuentes, J. D., do Vale, R. S., Alves, E. G., dos Santos, R. M. N., and Manzi, A. O.: Air turbulence characteristics at multiple sites in and above the Amazon rainforest canopy, *Agricultural and Forest Meteorology*, 260–261, 41–54, <https://doi.org/10.1016/j.agrformet.2018.05.027>, 2018.

- Schmitt, A. U., Ament, F., de Araújo, A. C., Sá, M., and Teixeira, P.: Modeling atmosphere–land interactions at a rainforest site – a case study using Amazon Tall Tower Observatory (ATTO) measurements and reanalysis data, *Atmospheric Chemistry and Physics*, 23, 9323–9346, <https://doi.org/10.5194/acp-23-9323-2023>, 2023.
- Serra-Neto, E. M., Martins, H. S., Dias-Júnior, C. Q., Santana, R. A., Brondani, D. V., Manzi, A. O., de Araújo, A. C., Teixeira, P. R., Sörgel, M., and Mortarini, L.: Simulation of the Scalar Transport above and within the Amazon Forest Canopy, *Atmosphere*, 12, 1631, <https://doi.org/10.3390/atmos12121631>, 2021.
- Silva Junior, C. H. L., Anderson, L. O., Silva, A. L., Almeida, C. T., Dalagnol, R., Pletsch, M. A. J. S., Penha, T. V., Paloschi, R. A., and Aragão, L. E. O. C.: Fire Responses to the 2010 and 2015/2016 Amazonian Droughts, *Front. Earth Sci.*, 7, <https://doi.org/10.3389/feart.2019.00097>, 2019.
- Stroud, C., Makar, P., Karl, T., Guenther, A., Geron, C., Turnipseed, A., Nemitz, E., Baker, B., Potosnak, M., and Fuentes, J. D.: Role of canopy-scale photochemistry in modifying biogenic-atmosphere exchange of reactive terpene species: Results from the CELTIC field study, *Journal of Geophysical Research: Atmospheres*, 110, <https://doi.org/10.1029/2005JD005775>, 2005.
- Sun, S., Moravek, A., Trebs, I., Kesselmeier, J., and Sörgel, M.: Investigation of the influence of liquid surface films on O<sub>3</sub> and PAN deposition to plant leaves coated with organic/inorganic solution, *Journal of Geophysical Research: Atmospheres*, 121, 14,239–14,256, <https://doi.org/10.1002/2016JD025519>, 2016.
- Unfer, G. R., Machado, L. A. T., Albrecht, R. I., Cecchini, M. A., Harder, H., Magina, F. C., Pöhlker, M. L., Pöschl, U., Vilà-Guerau de Arellano, J., Williams, E. R., Wolff, S., and Pöhlker, C.: Decoding the Relationship Between Cloud Electrification, Downdrafts, and Surface Ozone in the Amazon Basin, *Journal of Geophysical Research: Atmospheres*, 130, e2024JD042158, <https://doi.org/10.1029/2024JD042158>, 2025.
- Vermeuel, M. P., Millet, D. B., Farmer, D. K., Ganzeveld, L. N., Visser, A. J., Alwe, H. D., Bertram, T. H., Cleary, P. A., Desai, A. R., Helmig, D., Kavassalis, S. C., Link, M. F., Pothier, M. A., Riches, M., Wang, W., and Williams, S.: A Vertically Resolved Canopy Improves Chemical Transport Model Predictions of Ozone Deposition to North Temperate Forests, *Journal of Geophysical Research: Atmospheres*, 129, e2024JD042092, <https://doi.org/10.1029/2024JD042092>, 2024.
- Vieira, I., Verbeeck, H., Meunier, F., Peaucelle, M., Sibret, T., Lefevre, L., Cheesman, A. W., Brown, F., Sitch, S., Mbifo, J., Boeckx, P., and Bauters, M.: Global reanalysis products cannot reproduce seasonal and diurnal cycles of tropospheric ozone in the Congo Basin, *Atmospheric Environment*, 304, 119773, <https://doi.org/10.1016/j.atmosenv.2023.119773>, 2023.
- Visser, A. J., Ganzeveld, L. N., Goded, I., Krol, M. C., Mammarella, I., Manca, G., and Boersma, K. F.: Ozone deposition impact assessments for forest canopies require accurate ozone flux partitioning on diurnal timescales, *Atmospheric Chemistry and Physics*, 21, 18393–18411, <https://doi.org/10.5194/acp-21-18393-2021>, 2021.
- Visser, A. J., Ganzeveld, L. N., Finco, A., Krol, M. C., Marzuoli, R., and Boersma, K. F.: The Combined Impact of Canopy Stability and Soil NO<sub>x</sub> Exchange on Ozone Removal in a Temperate Deciduous Forest, *Journal of Geophysical Research: Biogeosciences*, 127, e2022JG006997, <https://doi.org/10.1029/2022JG006997>, 2022.
- Wang, C.-T., Campbell, P. C., Makar, P., Ma, S., Ivanova, I., Baek, B. H., Hung, W.-T., Moon, Z., Tang, Y., Baker, B., Saylor, R., Woo, J.-H., and Tong, D.: Quantifying forest canopy shading and turbulence effects on boundary layer ozone over the United States, *Atmospheric Chemistry and Physics*, 25, 16631–16655, <https://doi.org/10.5194/acp-25-16631-2025>, 2025.
- Wei, D., Alwe, H. D., Millet, D. B., Bottorff, B., Lew, M., Stevens, P. S., Shutter, J. D., Cox, J. L., Keutsch, F. N., Shi, Q., Kavassalis, S. C., Murphy, J. G., Vasquez, K. T., Allen, H. M., Praske, E., Crouse, J. D., Wennberg, P. O., Shepson, P. B., Bui, A. A. T., Wallace, H. W., Griffin, R. J., May, N. W., Connor, M., Slade, J. H., Pratt, K. A., Wood, E. C., Rollings, M.,

- Deming, B. L., Anderson, D. C., and Steiner, A. L.: FORest Canopy Atmosphere Transfer (FORCAsT) 2.0: model updates and evaluation with observations at a mixed forest site, *Geoscientific Model Development*, 14, 6309–6329, <https://doi.org/10.5194/gmd-14-6309-2021>, 2021.
- 1175 Wennberg, P. O., Bates, K. H., Crouse, J. D., Dodson, L. G., McVay, R. C., Mertens, L. A., Nguyen, T. B., Praske, E., Schwantes, R. H., Smarte, M. D., St Clair, J. M., Teng, A. P., Zhang, X., and Seinfeld, J. H.: Gas-Phase Reactions of Isoprene and Its Major Oxidation Products, *Chem. Rev.*, 118, 3337–3390, <https://doi.org/10.1021/acs.chemrev.7b00439>, 2018.
- Wesely, M. L.: Parameterization of surface resistances to gaseous dry deposition in regional-scale numerical models, *Atmospheric Environment* (1967), 23, 1293–1304, [https://doi.org/10.1016/0004-6981\(89\)90153-4](https://doi.org/10.1016/0004-6981(89)90153-4), 1989.
- 1180 Yan, X., Ohara, T., and Akimoto, H.: Statistical modeling of global soil NO<sub>x</sub> emissions, *Global Biogeochemical Cycles*, 19, <https://doi.org/10.1029/2004GB002276>, 2005.
- Yáñez-Serrano, A. M., Nölscher, A. C., Williams, J., Wolff, S., Alves, E., Martins, G. A., Bourtsoukidis, E., Brito, J., Jardine, K., Artaxo, P., and Kesselmeier, J.: Diel and seasonal changes of biogenic volatile organic compounds within and above an Amazonian rainforest, *Atmospheric Chemistry and Physics*, 15, 3359–3378, <https://doi.org/10.5194/acp-15-3359-2015>, 2015.
- 1185 Yáñez-Serrano, A. M., Nölscher, A. C., Bourtsoukidis, E., Gomes Alves, E., Ganzeveld, L., Bonn, B., Wolff, S., Sa, M., Yamasoe, M., Williams, J., Andreae, M. O., and Kesselmeier, J.: Monoterpene chemical speciation in a tropical rainforest: variation with season, height, and time of day at the Amazon Tall Tower Observatory (ATTO), *Atmospheric Chemistry and Physics*, 18, 3403–3418, <https://doi.org/10.5194/acp-18-3403-2018>, 2018.
- Yienger, J. and Levy, H.: Empirical model of global soil-biogenic NO<sub>x</sub> emissions, *Journal of Geophysical Research: Atmospheres*, 100, 11447–11464, 1995.
- 1190 Zhang, J., He, X., Ding, X., Yu, J. Z., and Ying, Q.: Modeling Secondary Organic Aerosol Tracers and Tracer-to-SOA Ratios for Monoterpenes and Sesquiterpenes Using a Chemical Transport Model, *Environ. Sci. Technol.*, 56, 804–813, <https://doi.org/10.1021/acs.est.1c06373>, 2022.

1195